NASA TECHNICAL NOTE

MEASUREMENTS OF SURFACE-PRESSURE AND WAKE-FLOW FLUCTUATIONS IN THE FLOW FIELD OF A WHITCOMB SUPERCRITICAL AIRFOIL

Frederick W. Roos and Dennis W. Riddle

Ames Research Center
Moffett Field, Calif. 94035

(53)

1. Report No. NASA TN D-8443	2. Government Accession No.	3. Recipient's Catalog No.
4. Title and Subtitle MEASUREMENTS OF SURFACE-PRESSURE AND WAKE-FLOW FLUCTUATIONS IN THE FLOW FIELD OF A WHITCOMB SUPERCRITICAL AIRFOIL*		5. Report Date August 1977
		6. Performing Organization Code
7. Author(s) Frederick W. Roos and Dennis W. Riddle		8. Performing Organization Report No. A-6877
		10. Work Unit No. 505-02-21
9. Performing Organization Name and Address McDonnell Douglas Research Lab. McDonnell Douglas Corp. St. Louis, Mo. 63166 and NASA Ames Research Center Moffett Field, Calif. 94035		11. Contract or Grant No.
		13. Type of Report and Period Covered Technical Note
12. Sponsoring Agency Name and Address National Aeronautics and Space Administration Washington, D.C. 20546		14. Sponsoring Agency Code

15. Supplementary Notes

*This research was conducted in part under the McDonnell Douglas Independent Research and Development Program.

16. Abstract

Measurements of surface-pressure and wake-flow fluctuations were made as part of a transonic wind-tunnel investigation into the detailed nature of a Whitcomb type supercritical airfoil flow field. Emphasis was on a range of high subsonic Mach numbers and moderate lift coefficients corresponding to the development of drag divergence and buffeting. Fluctuation data were analyzed statistically for intensity, frequency content, and spatial coherence; variations in these parameters were correlated with changes in the mean airfoil flow field.

Intense pressure fluctuations on the airfoil surface were related to the unsteadiness of primary shocks and "shocklets," and to trailing-edge flow separation. The primary upper surface shock increased the local intensity of pressure fluctuations throughout the range of frequencies considered, and regions of nearly sonic flow containing shocklets were characterized by concentrations of pressure-fluctuation energy in the higher frequencies. Wake downwash fluctuations showed a significant intensity increase across the frequency range upon the appearance of flow separation. Chordwise and spanwise coherences of fluctuations downstream of the primary upper surface shock were strong as long as the flow remained attached, but were greatly diminished with the onset of separation. The coherent pressure fluctuations in this region were propagated upstream.

17. Key Words (Suggested by Author(s)) Airfoil fluctuating pressures Airfoil fluctuating wakes Two-dimensional airfoils Supercritical airfoils		18. Distribution Statement Unlimited STAR Category — 02	
19. Security Classif. (of this report) Unclassified	20. Security Classif. (of this page) Unclassified	21. No. of Pages 53	22. Price* $4.25

Blank
Page

NOMENCLATURE

C_m fluctuating spanwise bending moment coefficient, $C_m = \dfrac{m_b}{M_b}$

C_p pressure coefficient, $C_p = \dfrac{p - p_\infty}{q_\infty}$

C_w downwash fluctuation coefficient, $C_w = \dfrac{w}{U_\infty}$

c airfoil chord, m (ft)

c_d airfoil section drag coefficient, $c_d = \dfrac{D}{q_\infty c}$

c_1 airfoil section lift coefficient, $c_1 = \dfrac{L}{q_\infty c}$

D airfoil drag per unit span, N/m (lb/ft)

f frequency, Hz

f_c frequency of characteristic fluctuations, Hz

L airfoil lift per unit span, N/m (lb/ft)

M Mach number

M_b mean spanwise bending moment, m-N (ft-lb)

m_b unsteady component of spanwise bending moment, m-N (ft-lb)

p static pressure, N/m^2 (lb/ft^2)

q free-stream dynamic pressure, $q_\infty = \dfrac{\rho_\infty U_\infty^2}{2}$, N/m^2 (lb/ft^2)

R_a autocorrelation coefficient for fluctuation $a(t)$, equation (3)

R_{ab} cross-correlation coefficient relating fluctuations $a(t)$ and $b(t)$, equation (6)

Re_c Reynolds number based on chord

t time, s

U_p streamwise disturbance propagation speed, m/s (ft/s)

U_∞ free-stream speed, m/s (ft/s)

u streamwise component of velocity fluctuation, m/s (ft/s)

w downwash component of velocity fluctuation, m/s (ft/s)

x coordinate in free-stream direction, m (ft)

y spanwise coordinate, m (ft)

z coordinate normal to free stream and span, m (ft)

α angle of attack, deg

γ^2_{ab} coherence function relating fluctuation $a(t)$ and $b(t)$, equation (8)

ΔC_p change of C_p across shock

ρ density, kg/m^3 (slugs/ft^3)

τ correlation time lag, s

ϕ_a power-spectral density of fluctuation $a(t)$, equation (4)

ϕ_{ab} cross-spectral density of fluctuations $a(t)$ and $b(t)$, equation (7)

ϕ' normalized power-spectral density, equation (5)

ω^* dimensionless frequency, $\omega^* = \dfrac{2\pi f c}{U_\infty}$

ω^*_c dimensionless frequency of characteristic fluctuation

Subscripts

l at lower edge of wake

max maximum

rms root-mean-square value, equation (1)

te at trailing edge

u at upper edge of wake

∞ free-stream value

MEASUREMENTS OF SURFACE-PRESSURE AND WAKE-FLOW FLUCTUATIONS

IN THE FLOW FIELD OF A WHITCOMB SUPERCRITICAL AIRFOIL*

Frederick W. Roos
McDonnell Douglas Corporation

and

Dennis W. Riddle
Ames Research Center

SUMMARY

Measurements of surface-pressure and wake-flow fluctuations were made
as part of a transonic wind-tunnel investigation into the detailed nature
of a Whitcomb type supercritical airfoil flow field. Emphasis was on a range
of high subsonic Mach numbers and moderate lift coefficients corresponding to
the development of drag divergence and buffeting. Fluctuation data were
analyzed statistically for intensity, frequency content, and spatial
coherence; variations in these parameters were correlated with changes
in the mean airfoil flow field.

Intense pressure fluctuations on the airfoil surface were related to the
unsteadiness of primary shocks and "shocklets," and to trailing-edge flow
separation. The primary upper surface shock increased the local intensity of
pressure fluctuations throughout the range of frequencies considered, and
regions of nearly sonic flow containing shocklets were characterized by
concentrations of pressure-fluctuation energy in the higher frequencies.
Wake downwash fluctuations showed a significant intensity increase across
the frequency range upon the appearance of flow separation. Chordwise and
spanwise coherences of fluctuations downstream of the primary upper surface
shock were strong as long as the flow remained attached, but were greatly
diminished with the onset of separation. The coherent pressure fluctuations
in this region were propagated upstream.

INTRODUCTION

This report deals with a portion of the problem of aircraft buffeting.
As used here, buffeting refers to the vibration, or mechanical oscillation,
that an aircraft in flight experiences when the airflow over its surfaces
becomes unsteady (because of flow separation, flow-field instability, or
free-stream unsteadiness). Buffeting has received the attention of aircraft

---

manufacturers and operators for more than 40 years, but the comparatively recent advent of aircraft that operate in, or very near, the transonic speed range is responsible for the present intensified interest.

Buffeting problems are most severe in the transonic speed range. This is so primarily because of the shock wave or waves that appear on surfaces of aircraft when mixed (subsonic and supersonic) flow exists. The difficulties are encountered both by high-performance military aircraft and by modern jet-powered transport aircraft.

Probably the most significant buffeting problem existing today is that limiting the transonic maneuverability of combat aircraft. The steep adverse pressure gradient associated with the upper wing surface shock in transonic flow tends to cause flow separation at values of section lift coefficient, c_l, considerably below the low-speed value of $c_{l_{max}}$; this in turn leads to severe buffeting at load factors well below any pilot- or airframe-imposed limitations. Because there generally exists a considerable range of increasing c_l (as a function of angle of attack) beyond the appearance of significant buffeting at transonic speeds, transonic maneuverability is, as a result, essentially buffet-limited.

On the other hand, subsonic transport aircraft, although not requiring high-speed maneuverability, do encounter buffeting as a result of flying at the high altitudes and high subsonic speeds necessary for efficient operation. Because their cruise speeds are very close to the drag-divergence boundary, which normally corresponds to the buffet boundary, these aircraft are prone to buffeting that may begin as a result of slight increases of lift or airspeed.

As was noted in a recent review of the fluid mechanics aspects of buffeting (ref. 1), very little is known about the structures of the unsteady flow fields responsible for buffeting. A considerable number of experimental investigations of buffeting response of specific configurations have been undertaken (e.g., refs. 2 and 3), and several parametric studies of airfoil-section (e.g., refs. 4 and 5) and wing (e.g., ref. 6) buffeting effects have been made. Likewise, efforts at analytical prediction of statistical aspects of airframe buffeting, begun by Liepmann (ref. 7), have continued, largely in the area of scaling wind-tunnel buffeting data to flight conditions (e.g., ref. 8). Only recently has any of this work given serious attention to details of the unsteady flow field (ref. 9), and then only the pressure fluctuations at a comparatively few points on the wing were measured and correlated.

Another recent development in transonic aerodynamics has been the advent of the rear-loaded, Whitcomb type supercritical airfoil for flight at high subsonic speeds (ref. 10). This airfoil has demonstrated a significant increase in drag-rise Mach number over that of conventional airfoils, and therefore shows great potential for improving transonic aircraft performance. Most of the effort that has gone into development of the Whitcomb type airfoil has been oriented toward specific applications with performance measurements (c_l, c_d, etc.) being the primary results.

.n the belief tnat a highly detailed experimental study of the flow field of a supercritical airfoil, focusing on the mechanisms of drag rise and buffet production, would be of substantial value in attempts to optimize the airfoil for various applications, a study was initiated by the McDonnell Douglas Research Laboratories (MDRL). An appreciable portion of the effort expended in this study was planned .o involve measuremen: and analysis of fluctuations in the airfoil flow field. While these measurements were intended to provide improved understanding of the development of flow unsteadiness, specifically for the Whitcomb type airfoil, it was felt that they would also be generally useful in expanding the understanding of transonic airfoil flow field dynamics in general.

A first series of transonic airfoil experiments was conducted in the McDonnell Douglas Corporation One-Foot Trisonic Wind Tunnel. Because the 5.08-cm (2-in.) chord airfoil model (McDonnell Douglas DSMA 523 section; essentially the Whitcomb airfoil of ref. 10) was too small to permit incorporation of instrumentation for nonsteady measurements, only wake fluctuations were measured in these tests. As reported in reference 11, the measurements related the transonic drag-rise phenomenon to large shock systems and trailing-edge separations, and to rapid increases in the intensities of velocity fluctuations in the airfoil wake.

The tests reported herein constituted a second phase of the transonic airfoil study, supported jointly by MDRL and Ames Research Center. Tests were run in the Ames 2- by 2-Foot Transonic Wind Tunnel, the airfoil model being of the same (DSMA ?3) section tested earlier, but this time with a 15.24-cm (6-in.) chord. .he greater model size permitted the inclusion of several high-frequency-response pressure transducers, as well as an expanded array of static pressure orifices. This added instrumentation was required to permit the airfoil flow field to be studied in the desired detail.

In addition to very detailed boundary-layer and wake-profile measurements and analyses, reported separately in reference 12, these experiments have provided heretofore unavailable information on the intensity, frequency content, and chordwise and spanwise coherence of pressure and velocity fluctuations in a supercritical airfoil flow field, and on the relationship of these fluctuations to the details of the mean flow field.

FACILITIES AND EQUIPMENT

Tests were performed in the 2- by 2-foot transonic wind tunnel at Ames Research Center, the test section having been modified by NASA for two-dimensional testing. The modified transonic test section retains the original slotted top and bottom walls; the side walls are unvented and incorporate rotatable, optical glass windows for supporting two-dimensional models.

The section shape of the tested airfoil model was a McDonnell Douglas profile, DSMA 523, which was essentially the original Whitcomb supercritical section (ref. 10) modified to include a trailing-edge thickness equal to

l-percent chord. Table 1 provides coordinates and an illustration of the
DSMA 523 section. Figure 1 shows a plan view of the stainless steel model,
indicating the instrumentation pertinent to the dynamic data experiments.
Pressures from the midspan row of 0.203-mm (0.008-in.) diameter static pres-
sure orifices were measured by a Scanivalve system. Thirteen miniature semi-
conductor strain-gage pressure transducers (for fluctuation measurements)
were embedded in the model; a strain-gage bridge circuit was installed to
permit monitoring of spanwise bending mode oscillations of the airfoil model.

The semiconductor strain-gage pressure transducers were buried within
the model rather than being flush-mounted, both for protection of the fragile
diaphragms and because there was insufficient model thickness at some
chordwise stations to permit flush-mounting. Employing a technique described
by Kendall (ref. 13), each transducer was fitted into a small aluminum cylin-
der in such a way that a minimum volume cavity provided communication between
the transducer diaphragm and the surface through a 1.016-mm (0.040-in.) diam-
eter orifice. The aluminum cylinder was set into the airfoil model, the
ported surface having been finished to the local model surface contour.
Figure 2 illustrates a typical transducer installation. The frequency
response of the transducers, as installed, was flat within 8 percent to
15 kHz.

Figure 3 shows the arrangement of the model and instrumentation in the
test section. A static-pressure-type probe, in which was installed another
pressure transducer, was attached to the test-section wall some distance
from the model for the purpose of monitoring background fluctuations in the
test section. A pair of crossed-sensor hot-film anemometer probes, each of
which had two cylindrical filaments inclined ±45° to the free stream (in
the vertical plane), was mounted on the MDRL-developed vertical traversing
rig downstream of the airfoil. (The traversing rig is described in more
detail in ref. 12.) These anemometer probes, the configuration of which
enabled the downwash component of flow velocity to be measured, were arranged
to "straddle" the (mean) wake, and were intended to sense overall large-scale
movements of the wake (rather than the small-scale turbulence within the
wake).

It is well known that the response of heated-sensor anemometers in
unsteady transonic flow is very complex; the complexity is a result of the
fact that the rate of heat transfer from the sensor is sensitive to fluctua-
tions in flow velocity, density, and stagnation temperature (ref. 14).
Consequently, the response of the type of crossed-sensor probe used in these
tests was evaluated carefully. One of the probes was thoroughly calibrated
over the ranges of Mach number, Reynolds number, and overheat ratio encountered
in the wind-tunnel tests, using a low-turbulence calibration jet arranged to
permit independent variations of Mach and Reynolds numbers. These calibration
data were used in conjunction with constant-temperature-anemometer sensitivity
expressions developed according to reference 15 and with reasonable estimates
of the nature of anticipated fluctuations (based on other experimental data)
to determine that less than 10-percent error resulted if the crossed-sensor
probe differential output were considered a function of downwash velocity
fluctuations alone.

Time-averaged data (including static pressures on the airfoil and the basic tunnel flow parameters) were acquired and recorded by the tunnel data system. The dynamic data were taken and recorded with a system furnished by Ames; the setup is illustrated in figure 4. Availability of 32 signal channels in the tape recorder allowed simultaneous recording of all fluctuating data. In order to permit calibration of the various track-to-track phase differences developed in the processes of recording and reproduction, each original 32-track data tape included a segment on which a sinusoidal calibration signal was simultaneously recorded on all 32 tracks.

Data reduction consisted of casting the time-averaged pressure and tunnel data into standard coefficient form, and statistically analyzing the dynamic data. Except for analog evaluation of root-mean-square (rms) levels of all fluctuations during the tests (these data later being used to check the results of other data reduction), all processing of dynamic data was done digitally. Standard techniques were employed (ref. 16): the signals were digitized from the FM tapes, auto- and cross-correlations were computed, and power- and cross-spectral densities were obtained by Fourier transformation of the correlations. Power-spectral density fluctuations were integrated to permit checking rms levels against the earlier analog results. Finally, in a number of cases, the cross spectra were converted into coherence function form.

RESULTS AND DISCUSSION

Mean Flow Field

The mean (i.e., time-averaged) flow field about the DSMA 523 airfoil has been described in detail in the companion to this report (ref. 12) and therefore is not covered at length here. It is appropriate, however, to characterize the overall mean flow field as affected by changes in M_∞ and c_1 through drag divergence/buffet onset.

Figures 5 and 6 show airfoil section pressure distributions as they evolve with increasing M_∞ and c_1, respectively. The baseline condition is taken to be $M_\infty = 0.82$, $c_1 = 0.56$. The noteworthy aspects of figure 5 are the constancy of the lower-surface pressure distribution, the rapid chordwise shift in shock location, and the nearly sonic flow downstream of the shock that exists for $M_\infty \leq 0.82$ but not for $M_\infty > 0.82$. The latter phenomenon is particularly important because the presence of nearly sonic mean flow permits upstream-propagating pressure disturbances to develop into shocklets during their relatively slow, and occasionally halted, passage over the rearward portion of the airfoil upper surface. (The shocklet phenomenon is described in the appendix.) This change from reaccelerated to decelerated flow downstream of the shock is even more clearly evident in the fixed M_∞ comparison of pressure distributions shown in figure 6. Also apparent here is a region of sonic flow near the nose on the lower surface; this sonic flow region disappears as c_1 is increased. Examination of pressures in the vicinity of the trailing edge indicates that the presence or absence of reacceleration aft of the shock is not directly associated with trailing-edge

separation. It is also clear that the reacceleration, or lack of it, is not simply related to the chordwise location of the shock. Whereas some of the pressure distributions in figures 5 and 6 exhibit features that are sometimes associated with shock-induced boundary-layer separation (on conventional airfoil sections), a thorough study of the pressure distributions, trailing-edge pressure recovery variations, and boundary-layer profiles for this air-foil (ref. 12) leaves no doubt that the upper surface boundary layer remained attached (except for the development of a trailing-edge-type separation at the highest c_l and M_∞ values).

Several spark Schlieren photographs at various M_∞, c_l combinations are given in figure 7. All but one of the photographs were taken at $Re_c = 3 \times 10^6$; the exception was taken at $Re_c = 2 \times 10^6$. The presence or absence of a pronounced system of shocklets on the rearward upper surface corresponds closely to the existence or nonexistence of reaccelerated flow (as indicated by the pressure distributions).

Fluctuation Intensities

Measured fluctuations were analyzed in three stages. The first step involved evaluation of the intensities of all fluctuations. The intensity, or root-mean-square (rms) level, of a fluctuation $a(t)$ is defined by

$$a_{rms} = \left[\lim_{T \to \infty} \frac{1}{T} \int_0^T a^2(t) dt \right]^{1/2} \tag{1}$$

Next, the frequency content of the fluctuations was established by the computation of power-spectral densities. Finally, cross-spectral densities and corresponding coherence functions were generated to provide information regarding the spatial relationships among the fluctuations.

Figure 8 illustrates the evolution of the upper surface fluctuating pressure distribution with increasing M_∞ (at fixed c_l). The shaded area in the $M_\infty - x/c$ plane corresponds to the chordwise "region" occupied by the shock, as defined by the pressure distributions. The most intense pressure fluctuations necessarily occur in this shock region; they are produced by chordwise oscillations of the shock. In a few cases, where the shock was positioned directly over a pressure transducer, this maximum level of $C_{p_{rms}}$ was actually measured. In all other cases, the peak was "constructed" by assuming the pressure fluctuation intensity to scale with the overall pressure rise through the shock. The experimentally determined scaling factor was approximately 1/6; that is,

$$\left(C_{p_{rms}} \right)_{shock} \approx \frac{1}{6} \left(\Delta C_p \right)_{shock} \tag{2}$$

For the pressure distributions in figure 4, the shock ΔC_p is seen to be in the range of 0.4 to 0.5, with most of the values closer to 0.4. According

6

to equation (2), this corresponds to $\left(C_{p_{rms}}\right)_{shock} = 0.07$, approximately the peak level shown in figure 8.

Also evident in figure 8 is the low $C_{p_{rms}}$ level forward of the shock, particularly when the shock is well aft on the airfoil.[1] In contrast, the rms level is much higher downstream of the shock. At the lower Mach numbers ($M_\infty < 0.82$), the C_p fluctuations are rather intense between the shock and the trailing edge, decreasing toward the latter. This M_∞ range corresponds to the existence of nearly sonic flow downstream of the shock, the intense pressure fluctuations being associated with the formation and passage (upstream) of the shocklets mentioned earlier. As M_∞ is increased above 0.82, this phenomenon disappears and the pressure fluctuation intensity decreases correspondingly. Trailing-edge flow separation appears as M_∞ increases above 0.84, producing a pronounced increase in $C_{p_{rms}}$ near the trailing edge.

Several variables are plotted against increasing M_∞ in figure 9. It is well established (e.g., ref. 11) that divergence of the trailing-edge pressure coefficient $(C_{p_{te}})$ is associated with drag divergence. Because direct drag measurements could not be made in these tests, $C_{p_{te}}$ is used to signal drag divergence/buffet onset. Clearly, both $C_{p_{rms}}$ at 90-percent chord[2] and the downwash fluctuation intensity $(C_{w_{rms}})$ at the upper edge of the wake were strong indicators of drag divergence; the other variables were ambiguous (e.g., $C_{p_{rms}}$ at 80-percent chord) or even deceptive (e.g., $C_{p_{rms}}$ at 10-percent chord, lower surface) as drag-divergence indicators.

The pronounced difference between pressure fluctuation intensities at 10-percent chord on the upper and lower surfaces should be noted. This again involves the condition of nearly sonic flow and the associated presence of a system of moving shocklets (evident in figs. 5 and 7, respectively). As the C_p distributions in figure 5 reveal, the situation in the vicinity of 10-percent chord on the lower surface is different at the highest Mach number; that is, the local flow is decidedly supersonic. Correspondingly, the unsteady shocklets disappear (fig. 7(f)) and $C_{p_{rms}}$ drops appreciably (fig. 9).

Figure 10 shows again the evolution of the chordwise $C_{p_{rms}}$ distribution, as affected by increasing c_l. Although the chordwise shift of the shock is not so great in this case, the overall trend with increasing c_l is

---

[1]It should be noted that the pressure fluctuation levels forward of the upper surface shock were comparable to the "background" fluctuation level measured by the monitoring probe shown in figure 3. It is likely that pressure fluctuation levels measured ahead of the shock on a wing in flight would be lower than these values.

[2]Chordwise locations of measurements always refer to the upper surface unless specifically identified otherwise.

similar to the variation with increasing M_∞. In particular, the change with increasing c_l from shocklet-produced intense pressure fluctuations aft of the shock to low $C_{P_{rms}}$ levels to separation-induced pressure fluctuations is readily apparent.

The change in several variables with increasing c_l is shown in figure 11. Once again it is evident that $C_{P_{rms}}$ at 90-percent chord and $C_{u_{rms}}$ successfully indicate drag divergence (as signaled by the $C_{P_{te}}$ break), while the other variables do not.

Frequency Distribution of Fluctuations

Since the objective of these tests was the study of buffeting rather than turbulence, attention was concentrated on low frequencies (associated with large spatial scales). In general, spectral analyses were limited to frequencies below 2 kHz, corresponding to ω^* less than about 8 (this covered the dimensionless frequency range normally considered in buffeting of full-scale aircraft, e.g., ref. 17); in a few cases, the frequency range was extended by an order of magnitude.

Power-spectral densities were computed digitally, with a normalized *rms* error of approximately 25 percent. The traditional procedure was used, with the autocorrelation computed from the digitized raw data and the power-spectral density then evaluated by Fourier transformation of the autocorrelation. For a fluctuating quantity $a(t)$, the relationships are (after ref. 16) the autocorrelation coefficient,

$$R_a(\tau) = \frac{1}{a_{rms}^2} \lim_{T \to \infty} \frac{1}{T} \int_0^T a(t)a(t + \tau)dt \tag{3}$$

and the power-spectral density,

$$\phi_a(\omega^*) = \frac{2}{\pi} C_{a_{rms}}^2 \int_0^\infty R_a(\tau) \cos \frac{\omega^* U_\infty \tau}{c} \, d\left(\frac{U_\infty \tau}{c}\right) \tag{4}$$

It can readily be shown that

$$\int_0^\infty \phi_a(\omega^*)d\omega^* = C_{a_{rms}}^2$$

where $C_{a_{rms}}$ is the *rms* value of the appropriate coefficient of $a(t)$, e.g., $C_{P_{rms}}$ for pressure fluctuations. The normalized power-spectral density ϕ_a' is defined to be

$$\phi'_a(\omega^*) = \frac{\phi_a(\omega^*)}{C^2_{a_{rms}}}$$

(5)

so that

$$\int_0^\infty \phi'_a(\omega^*)d\omega^* = 1$$

The first point to be emphasized in discussing the frequency content of the fluctuations is that the mechanical vibrations and aerodynamic unsteadiness were indeed independent. This is apparent in figure 12, where power-spectral densities of several unsteady variables are compared for a typical test. The bending moment power spectrum shows a pronounced peak at the resonant frequency for the fundamental spanwise bending mode. The unsteady aerodynamic variables measured on or near the airfoil (pressures at 10-percent and 90-percent chord, and downwash velocity at the edge of the airfoil wake) show definite peaks at a common frequency (110 Hz) that is clearly distinct from the bending vibration frequency (80 Hz). Evident from the spectra of figure 12 is the absence of any significant interaction of these two unsteady phenomena. Another important point is the absence of a peak at either of the noted frequencies in the power spectrum of pressure fluctuations at the monitoring probe; this absence indicates that neither fluctuation produced a sensible effect away from the immediate vicinity of the airfoil (and its wake).

Unfortunately, a vibration test of the installed airfoil model was not performed. Although estimates were made of the frequencies corresponding to torsional vibrations and rigid body pitching oscillations of the airfoil, neither of these being identifiable with the 110-Hz spectral peaks, an aerodynamic-mechanical interaction cannot be entirely ruled out as the source of the 110-Hz fluctuations. This possibility has been strengthened somewhat by more recent tests (still being analyzed), which show noticeably less pronounced spectral peaks in the vicinity of 110 Hz.

The shape of the fluctuating surface-pressure power spectrum is strongly influenced both by the shock on the upper surface and by the C_p distribution between the shock and the trailing edge. Unfortunately, it is not possible to completely separate the two effects; however, comparative study of upper surface-pressure power spectra does help define the two influences.

Pressure spectra measured at four chordwise stations on the airfoil are compared in figure 13; the spectra are for a flow condition representing the nominal lift coefficient and a pre-drag-divergence Mach number. The spectrum at 10-percent chord is representative of that station under all flow conditions studied; the uniform logarithmic decrease of power-spectral density (ϕ_p) with increasing frequency is typical of all spectral densities upstream of the shock region. At 40-percent chord, the transducer was within the chordwise region occupied by the mean shock-wave pressure rise, and ϕ_p at that station exhibits the somewhat surprising fact that the local effect of the shock is to intensify pressure fluctuations at all frequencies (within

9

the range investigated), rather than to produce a discrete-frequency or narrow-band effect. Similar results have been observed in NASA studies of pressure fluctuations associated with ramp- and step-induced separation of supersonic turbulent boundary layers (ref. 18). Downstream of the shock, in the nearly sonic reaccelerated flow region, ϕ_p at 70-percent chord shows a pronounced shift of fluctuating pressure energy from frequencies below $\omega^* \approx 0.8$ to higher frequencies. Finally, in the midst of the steeply adverse pressure gradient approaching the trailing edge, ϕ_p at 90-percent chord has a much slower rate of decline with increasing ω^* than does ϕ_p anywhere upstream of the shock. As will be shown, this spectral shape is very characteristic of the 90-percent station and is independent of the shock position and the presence or absence of reacceleration downstream of the shock. It is interesting to note that a definite peak exists at $\omega^* \approx 0.4$ in the spectra measured at 10-percent and 90-percent chord, but not in the other spectra. Another peak, at $\omega^* \approx 0.66$, occurs in the spectra at, and downstream of, the shock. The former unsteady phenomenon appears to be associated with the overall airfoil flow field, while the latter is a local oscillation (found neither forward on the airfoil nor in the wake).

A post-drag-divergence comparison of pressure spectra appears in figure 14; there the frequency range has been extended by an order of magnitude beyond the usual upper limit. Except in the vicinity of $\omega^* \approx 0.4$, the spectra at 10-percent and 40-percent chord are quite similar. The 70-percent chord spectrum, from the upstream end of the shock region, shows the typical increase of ϕ_p at all frequencies. The spectrum at 90-percent chord again shows its typical shape and level, in spite of the different conditions; it shows no reacceleration of the flow downstream of the shock and shows the existence of boundary-layer separation ahead of the trailing edge (as is indicated by the $C_{p_{te}}$ curve in fig. 9).

The final chordwise comparison of pressure spectra, that of figure 15, corresponds to a flow condition well into the drag rise. Once again the spectra upstream of the shock are characteristic of that region (and again the spectral peak at $\omega^* \approx 0.4$ does not appear in ϕ_p at 55-percent chord). In this case, the shock region occurred directly over the pressure transducer at 70-percent chord, and the spectrum correspondingly shows a pronounced increase in level across the frequency range, although the intensification is clearly less at the higher frequencies. Despite the extensive trailing-edge boundary-layer separation (the C_p distribution in fig. 5 indicates that separation occurs at about 80-percent chord), ϕ_p at 90-percent chord remains very similar to spectra measured at that station with attached flow.

Figures 16-19 present an alternative comparison of fluctuating pressure power spectra by showing the variation with changing flow conditions of spectra measured at a fixed chordwise station. The spectra in figure 16 were taken at 40-percent chord and are compared in terms of the relative positions of the shock and the transducer. When the shock was 0.25c downstream of the transducer, the spectrum showed the characteristic logarithmic form with a slope

$$\frac{\partial \ln \phi_p}{\partial \ln \omega^*} \cong -\frac{5}{4}$$

When the shock was directly over the measuring station, ϕ_p was increased substantially across the range of ω^*. The spectrum produced when the shock was 0.18c upstream of 40-percent chord is typical of the flow aft of the shock in cases where reacceleration to nearly sonic conditions occurred. Although in the present case the flow beyond the shock was decidedly subsonic in the mean (M_∞ = 0.749 pressure distribution in fig. 5), the shocklets associated with nearly sonic flow were definitely present (fig. 7(a)); apparently these shocklets are largely responsible for the altered shape of the power spectrum.

Figure 17 represents spectra from the transducer at 70-percent chord. These spectra detail the local effect of the shock on the fluctuating pressure power spectrum; three of the spectra correspond to slight shifts of the shock position in the immediate vicinity of 70-percent chord. In the case when the shock is 0.05c downstream of 70-percent chord, the spectrum shows the typical steep falloff that is characteristic of the supersonic region upstream of the shock, somewhat modified by the proximity of the shock. When the shock was directly over the transducer, the spectrum shape is little changed while the level is greatly raised. When the shock is 0.05c upstream of the 70-percent chord station, the overall level of ϕ_p is again down, but the rate at which ϕ_p diminishes with increasing ω^* is clearly lower than for the case when the shock was 0.05c. Finally, with the shock positioned 25-percent chord upstream of the transducer, the flow is sonic at 70-percent chord and the spectrum exhibits the corresponding shift of energy toward the higher frequencies.

The comparison of spectra from the 80-percent chord transducer, given in figure 18, accentuates the influence of the pressure distribution downstream of the shock; the shock is more than 0.05c upstream of 80-percent chord in all cases. The overall impression given by this comparison is clearly that, as the flow downstream of the shock evolves from the reaccelerated, nearly sonic case into the case where C_p continues to rise rapidly from the shock to the trailing edge, the ϕ_p distribution changes from one in which energy is concentrated at $\omega^* > 0.8$ into one that is essentially monotonically decreasing (except for the narrow-band peak at $\omega^* \approx 0.4$).

The final comparison of fluctuating pressure power spectra concerns measurements made at 90-percent chord. These spectra, shown in figure 19, clearly illustrate that $\phi_{p_{90\%c}}$ is significantly affected only by the extent of boundary-layer separation near the trailing edge; the presence or absence of flow reacceleration downstream of the shock has little bearing on either the shape or the level of the power spectrum at 90-percent chord.

In contrast with the great variation in levels and shapes of power spectra on the upper airfoil surface associated with the variety of C_p distributions produced by the different flow conditions, the relatively unchanging

11

lower surface C_p distribution (especially aft of about 50-percent chord — refer to figs. 5 and 6) resulted in comparatively little variation of the lower surface power spectra. In fact, ϕ_p was nearly invariant at both 55-percent and 90-percent chord on the lower surface, the spectra at each station falling almost entirely within a ±50-percent band along an average ϕ_p curve. The spectra at 10-percent chord on the lower surface showed somewhat greater variation because of the changes in the unsteady shocklet aspect of the local flow. Representative fluctuating pressure power spectra from the three lower surface transducers are presented in figure 20 for a typical flow condition. The spectra at 10-percent and 55-percent chord both show the energy shift to higher frequencies associated with the presence of moving shocklets at those locations, while the spectrum at 90-percent chord is quite similar (but not identical) to those measured at the same station on the upper surface, the flows having undergone substantial recompressions in both cases.

Although the overall intensity of velocity fluctuations at the upper edge of the airfoil wake varied greatly according to flow conditions (as was shown in figs. 9 and 11), the shapes of the power spectra of the unsteady streamwise and downwash velocity components (u_u, w_u) are remarkably similar. This is evident in figure 21 which gives the envelopes of the normalized u_u and w_u spectra. It is rather surprising, at least in this range of ω^*, that the development of an extensive region of separated flow near the upper surface trailing edge (at the higher M_∞, c_l values) has no effect on the spectral shapes. A further point to note in figure 21 is the pair of pronounced spectral peaks at $\omega^* \approx 0.4$ and $\omega^* \approx 0.8$, the latter being precisely the first harmonic of the former.

An obvious feature of the majority of power spectra included in this report is the pronounced peak at $\omega^* \approx 0.4$. Although the frequency ω_c^* associated with this narrow band peak appears to be constant, it actually demonstrates a slight well defined Mach number dependence, as indicated in figure 22. Also shown is the curve that would result if the dimensional frequency, f_c, were truly constant. The phenomenon responsible for this fluctuation is not clearly understood; it will be discussed at greater length following the next section.

Coherence of Fluctuations

This section deals with the coherence, or spatial organization, of the fluctuations in the airfoil flow field. The spatial coherence of pressure fluctuations on the airfoil surface is important because the buffeting, or response of the structure to these pressure fluctuations, depends largely on the extent of surface area over which the fluctuations are correlated. The results presented here are primarily cast into the form of coherence functions.

The coherence function is the ratio of the square of the magnitude (modulus) of the cross-spectral density function to the product of the two associated power-spectral densities. It serves to present, in frequency-resolved terms, the extent of the correlation between two fluctuating variables

(without concern for phase relationships). The necessary relationships (ref. 16) for two fluctuations $a(t)$ and $b(t)$ are the cross-correlation coefficient,

$$R_{ab}(\tau) = \frac{1}{a_{rms} b_{rms}} \lim_{T \to \infty} \int_0^T a(t)b(t + \tau)dt \tag{6}$$

and the cross-spectral density,

$$\phi_{ab}(\omega^\star) = \frac{1}{\pi} C_{a_{rms}} C_{b_{rms}} \int_\infty^\infty R_{ab}(\tau) e^{-i(\omega^\star U_\infty \tau/c)} \, d\left(\frac{U_\infty \tau}{c}\right) \tag{7}$$

Because the cross correlation is generally not symmetrical about $\tau = 0$, the cross-spectral density has real and imaginary parts. This can be expressed by

$$\phi_{ab}(\omega^\star) = C_{ab}(\omega^\star) - iQ_{ab}(\omega^\star)$$

$$= |\phi_{ab}(\omega^\star)| e^{-\Theta_{ab}(\omega^\star)}$$

where

$$|\phi_{ab}(\omega^\star)| = \left[C_{ab}^2(\omega^\star) + Q_{ab}^2(\omega^\star) \right]^{1/2}$$

and

$$\Theta_{ab}(\omega^\star) = \tan^{-1}\left[\frac{Q_{ab}(\omega^\star)}{C_{ab}(\omega^\star)} \right]$$

Finally, the coherence function is

$$\gamma_{ab}^2 = \frac{|\phi_{ab}|^2}{\phi_a \phi_b} \tag{8}$$

Figure 23 shows that the unsteady pressures at 80-percent and 90-percent chord on the airfoil upper surface are highly coherent over most of the frequency range considered, as long as the flow remains attached back to the trailing edge. The development of significant upper surface flow separation sharply reduces the coherence; in the highest Mach number case ($M_\infty = 0.866$, $c_l = 0.458$), for which separation occurs at about 85-percent chord, the coherence is almost negligible.

The velocities labeled U_p in figure 23 are the average streamwise velocities of propagation of the coherent pressure disturbances, as indicated by the phase lag versus frequency plots corresponding to the coherence functions. The negative values indicate that the significant pressure fluctuations are propagated upstream. In fact, this is the case whenever the

13

flow remains attached all the way to the trailing edge; pressure fluctuations downstream of the shock are intense, well correlated, and propagated upstream. This is illustrated in figure 24, which shows how the unsteady pressure at 90-percent chord correlates with pressure fluctuations at stations upstream for a typical flow condition (recalling from fig. 5 that the shock occurs in the vicinity of 40-percent chord). The unsteady pressures are clearly correlated throughout the region between the shock and the trailing edge, and the negative value of τ at the correlation peak in each case corresponds to upstream propagation. Recall from the discussion of pressure-fluctuation intensities that the formation and upstream propagation of a system of shocklets is considered to be responsible for the intense pressure fluctuations aft of the shock; the present results arise from the same shocklet propagation phenomenon. Although there were too few pressure transducers on the lower surface for appropriate measurements, similar results would likely be obtained in the shocklet region on the forward lower surface.

Although pressure fluctuations are generally much less intense over the forward half of the upper surface, compared with those near the trailing edge, there is still appreciable coherence. Figure 25 is a comparison of coherence functions for pressures measured at 40-percent and 55-percent chord.[3] It is interesting to note that when the shock is well upstream of 40-percent chord (i.e., when $M_\infty = 0.749$), pressure fluctuations at 40-percent and 55-percent chord are strong (fig. 8) and almost completely correlated for frequencies between 100 and 800 Hz; when the shock is downstream of 55-percent chord ($M_\infty = 0.821$), the much weaker pressure fluctuations show coherence primarily at higher frequencies. A further increase of M_∞ to 0.83 causes the coherence to disappear almost completely.

Except when the shock lies between the transducers, in which case the fluctuations are 180° out-of-phase, the disturbances appear to be propagated upstream. This is clearly so when the shock is completely upstream ($M_\infty = 0.749$ case), according to the mechanism that has been discussed. However, there is also evidence of upstream propagation forward of the shock, where the flow is supersonic.

The mechanism responsible for this is wave propagation in the subsonic outer flow. As a pressure wave travels upstream around the supersonic region, it propagates obliquely across the supersonic zone, creating an upstream-running "footprint" on the airfoil surface. It follows that the "strength" of the upstream propagation indicated in this region by the surface pressure fluctuations should diminish as the supersonic zone grows (with increasing M_∞ and/or α_1); this argument is substantiated by the experimental data.

Pressure fluctuations around the airfoil leading edge are very coherent at low frequencies, as figure 26 indicates. Here the cross-spectral density modulus is also shown for the two cases to indicate where the fluctuation

---

[3] The coherence peaks occurring at $f = 1300$ Hz result from a fan-generated tunnel disturbance.

energy is concentrated (i.e., in the peaks at $f_c \doteq 110$ Hz). The phase plots (not shown) reveal that the fluctuations at 10-percent chord on the upper and lower surfaces are 180° out of phase.

An effort was made to evaluate the correlation between large-scale fluctuations of the airfoil wake and the unsteady pressure field acting on the airfoil. Downwash fluctuations at the upper edge of the wake and pressure fluctuations at 90-percent chord were essentially incoherent except at low frequencies and in a few narrow frequency bands (fig. 27). The frequencies primarily involved were f_c and its first harmonic, $2f_c$. The low-frequency-band coherence tended to diminish with increasing c_l or M_∞, particularly the latter. Coherence at f_c and $2f_c$ remained strong with increasing c_l but diminished as M_∞ increased. Unfortunately, a propagation direction for the f_c disturbance could not be established; the possibility exists that the disturbance might originate at the trailing edge, simultaneously propagating forward as a pressure wave and being convected downstream as a velocity disturbance in the wake. (The phenomenon responsible for f_c is not classical vortex shedding from the blunt trailing edge of the airfoil, since the frequency of such shedding would be almost two orders of magnitude greater than f_c.)

In connection with the wake, it was interesting to note that the only significant coherence across the wake (vertically) occurred at f_c. This is evident in the two parts of figure 28, which show the coherence function and cross-spectral density modulus relating the unsteady downwash measurements at the upper (w_u) and lower (w_l) edges of the wake. The coherence levels at f_c and $2f_c$ remained nearly constant for all c_l and for all $M_\infty > 0.80$. Phase measurements indicate that w_u and w_l are essentially in phase at f_c and $2f_c$. Hence, the fluctuations amount to a vertical undulation or flapping of the wake.

Figure 29 indicates the spanwise coherence of pressure fluctuations at 90-percent chord. The upper plot, representing a typical attached flow situation, indicates appreciable spanwise coherence at frequencies above 150 Hz. The upper limit to the coherence range scales roughly with the inverse of the spanwise transducer spacing, which suggests that higher disturbance frequencies correspond to shorter spatial scales. The lower plot in figure 29 compares coherences among the same set of transducers in a case with flow separation at about 85-percent chord. Clearly, the coherence has disappeared. The only real surprise in figure 29 is the absence of any coherence at f_c in the attached flow case. Examination of the individual power-spectral densities revealed that the fluctuation at f_c simply did not exist at the transducer offset by 50-percent chord (in the spanwise direction), and appeared only marginally at the transducer 15-percent chord away. Downwash fluctuation measurements at the upper edge of the wake did show noticeable coherence at f_c when the two anemometer probes were separated spanwise by 15-percent chord.

The Characteristic Frequency

The repeated occurrence, throughout most of the airfoil flow field and under most of the test conditions, of fluctuations with a characteristic frequency of $\omega_C^* = 0.4$ has already been noted. Because these fluctuations appeared primarily in areas of low-intensity pressure fluctuations (e.g., the noise region and forward upper surface of the airfoil), they were not believed to be particularly important with regard to the generation of airfoil buffeting. Nevertheless, because they constituted a prominent aspect of the unsteady flow field, an attempt was made to identify their origin.

A check of data from the unsteady static-pressure monitoring probe attached to the test-section wall confirmed that no detectable spectral peak existed at ω_C^*. In addition, hot-film anemometer data taken in the clean test section (airfoil model not installed) were analyzed with the same result. Thus, the characteristic fluctuation does not appear to be the result of pressure- or vorticity-type disturbances in the tunnel. It should also be recalled that the ω_C^* fluctuations were found not to be associated with spanwise bending vibrations of the airfoil model (fig. 12), although the possible existence of some other aerodynamic-mechanical interaction could not be positively ruled out.

Primarily because of the very low frequency involved, it was thought to be extremely unlikely that any kind of boundary-layer-scale disturbance could have produced the ω_C^* fluctuations.

The tentative hypothesis proposed to explain ω_C^*, then, is that the ω_C^* fluctuations resulted from lift fluctuations and associated unsteady chordwise movements of the upper surface shock. The loop may have been closed by the shocklets that run upstream from the trailing edge to the shock. This suggested hypothesis is consistent with several observed features of the ω_C^* fluctuations, namely: (1) where they existed, fluctuations at ω_C^* generally were well correlated; (2) the ω_C^* phenomenon involved fluctuations of the overall downwash aft of the trailing edge; and (3) ω_C^* fluctuations invariably showed a phase reversal across the upper surface shock.

CONCLUDING REMARKS

A series of experiments was performed in which fluctuating pressures and velocities on and about a DSMA 523 supercritical airfoil section were measured for a number of c values and several Mach numbers in the transonic range. Analysis of the measured data has led to a number of observations and conclusions regarding the development of flow field unsteadiness with variations of c and M_∞ in the range of drag divergence and buffet onset.

1. Intense pressure fluctuations on the airfoil surface arise from one of three causes: (a) unsteady chordwise movement of the shock wave, (b) development and propagation of shocklets in regions of nearly sonic flow, and (c) the existence of flow separation. Generally, pressure fluctuation

intensities were low ($C_{p_{rms}} \approx 0.01$) upstream of the upper surface shock; they were high ($C_{p_{rms}} \approx 0.06$ to 0.08) under the shock; and they diminished to an intermediate level ($C_{p_{rms}} \approx 0.03$ to 0.04) downstream of the shock, this level resulting from either (b) or (c). Pressure fluctuation intensities on the lower surface were low ($C_{p_{rms}} \approx 0.015$ to 0.02) except near the leading edge, where a region of shocklets normally existed ($C_{p_{rms}} \approx 0.03$).

2. Downwash-type velocity fluctuations, measured at the upper edge of the airfoil wake downstream of the trailing edge, showed a rapid rise in intensity when flow separation (associated with drag divergence) developed.

3. The frequency distribution of the pressure fluctuation energy is strongly influenced by both the shock and the overall C_p distribution. Upstream of the shock, the pressure power spectrum declines logarithmically with a slope of approximately -5/4. The presence of the shock raises ϕ_p across the spectrum while generally maintaining the shape and slope. Reaccelerated or nearly sonic flow downstream of the shock produces a significant shift of energy to frequencies above $\omega^* \approx 0.8$. Near the trailing edge, the pressure spectrum again becomes logarithmic, but with a less steep slope; the existence of trailing-edge separation distorts the higher frequency end of the spectrum.

4. Power spectra of wake fluctuations change in overall magnitude but not in shape as the overall intensity varies.

5. Chordwise and spanwise coherences of pressure fluctuations downstream of the upper surface shock are high as long as the flow remains attached, but are reduced drastically upon the development of trailing-edge flow separation. The coherent pressure fluctuations in this region are propagated upstream and thus are associated with the system of shocklets.

6. The airfoil wake executes undulating motions that are correlated with fluctuations of pressure on the airfoil upper surface near the trailing edge; this coherence is diminished as flow separation develops.

Ames Research Center
    National Aeronautics and Space Administration
        Moffett Field, Calif. 94035, January 13, 1977.

APPENDIX

THE SHOCKLET PHENOMENON

The term "shocklet" has been employed in this report to describe upstream-propagating pressure waves of finite intensity. These waves, which appear in the nearly sonic portions of the airfoil flow field, originate in the trailing-edge/near-wake region. They begin as acoustic disturbances associated with wake fluctuations or vortex shedding. In the latter connection, the phenomenon corresponds to one treated by Davis (ref. 19), except that the vortex shedding in the present case is random instead of periodic.

The upstream progress of these waves is greatly retarded by the speed of the flow into which the waves are propagating. Not only is the free-stream flow speed approaching the sonic range ($0.75 < M_\infty < 0.87$ in these experiments), but, in the cases where shocklets appear, the local flow downstream of the shock on the airfoil upper surface is nearly sonic. Consequently, the time required for passage of these waves from the trailing edge forward to the shock is very great compared with a characteristic acoustic time (e.g., c/a_∞), sufficiently great in fact to allow the waves to steepen into finite pressure fronts, and to permit successive waves to coalesce into even stronger waves. This is comparable to the wave propagation phenomenon described by Tijdeman and Zwaan (ref. 20) in the case of control-surface oscillation on a transonic airfoil, although the present case again differs in that the disturbance is random rather than periodic. It also differs in that there is some random unsteadiness to the overall airfoil flow field in which the shocklets are propagating.

The shocklet phenomenon possesses three characteristic features: (1) because the waves have finite pressure and density changes associated with them, they show up clearly in spark Schlieren photographs (fig. 7); (2) for the same reason, they also produce rather intense pressure fluctuations on the airfoil surface (figs. 8 and 10); and (3) since the shocklets are passing upstream, two-point pressure correlations show peaks corresponding to upstream propagation (fig. 24). While downstream acoustic propagation and convection of boundary-layer-induced pressure fluctuations also exist, the pressure fluctuations associated with the shocklets greatly predominate.

REFERENCES

1. Roos, F. W.: Fluid Mechanics Related to Airfoil Buffeting: A Review. McDonnell Douglas Report MDC Q0456, Dec. 1971.

2. Hollingsworth, E. G.; and Cohen, M.: Determination of F- Aircraft Transonic Buffet Characteristics. J. Aircraft, vol. 8, no. 10, 1971, pp. 757-763.

3. Damstrom, E. K.; and Mayes, J. F.: Transonic Flight and Wind Tunnel Buffet Onset Investigation of the F-8D Aircraft — Analysis of Data and Test Techniques. AIAA Paper 70-341, March 1970.

4. Polentz, Perry P.; Page, William A.; and Levy, Lionel L., Jr.: The Unrteady Normal-Force Characteristics of Selected NACA Profiles at High Subsonic Mach Numbers. NACA RM A55C02, 1955.

5. Coe, Charles F.: A Study of Local-Pressure Fluctuations Relative to Static-Pressure Distributions on Two-Dimensional Airfoils at High Subsonic Mach Numbers. NACA RM A55J11, 1955.

6. Ray, Edward J.; and Taylor, Robert T.   Buffet and Static Aerodynamic Characteristics of a Systematic S   s of Wings Determined from a Subsonic Wind-Tunnel Study. NASA TN D-5805, 1970.

7. Liepmann, H. W.: On the Application of Statistical Concepts to the Buffeting Problem. J. Aeron. Sci., vol. 19, no. 12, 1952, pp. 793-800, 822.

8. Huston, Wilbur B.: A Study of the Correlation Between Flight and Wind Tunnel Buffet Loads. Report 111, AGARD, 1957.

9. Mullans, R. E.; and Lemley, C. E.: Buffet Dynamic Loads During Transonic Maneuvers. AFFDL-TR-72-46, McDonnell Aircraft Co., 1972.

10. Whitcomb, Richard T.: Basic Results of a Wind-Tunnel Investigation of an Integral (Unslotted) Supercritical Airfoil Section. NASA LWP-505, 1967.

11. Hurley, F. X.; and Roos, F. W.: Experimental Study of the Flow Field About an Advanced Transonic Airfoil. McDonnell Douglas Report MDC Q047, Dec. 1973.

12. Hurley, F. X.; Spaid, F. W.; Roos, F. W.; Stivers, L. S., Jr.; and Bandettini, A.: Detailed Transonic Flow Field Measurements About a Supercritical Airfoil Section. NASA TM X-3244, 1975.

13. Kendall, David N.: Application of Miniature Pressure Transducers to the Measurement of Buffet Phenomena. Paper presented at 17th Aerospace Instrumentation Symposium, Inst. Soc. Am., Las Vegas, Nev.   y 1971.

14. Morkovin, Mark V.: Fluctuations and Hot-Wire Anemometry in Compressible
       Flows. AGARDograph 24, 1956.

15. Sandborn, Virgil A.: Resistance Temperature Transducers. Metrology
       Press, Fort Collins, Colo., 1972, chapter VII.

16. Bendat, Julius S.; and Piersol, Allan G.: Random Data: Analysis and
       Measurement Procedures. Wiley-Interscience, 1971.

17. Benepe, D. B.; Cunningham, A. M., Jr.; and Dunmeyer, W. D.: A Detailed
       Investigation of Flight Buffeting Response at Subsonic and Transonic
       Speeds. AIAA Paper 74-358, April 1974.

18. Coe, C. F.; Chyu, W. J.; and Dods, J. B., Jr.: Pressure Fluctuations
       Underlying Attached and Separated Supersonic Turbulent Boundary
       Layers and Shock Waves. AIAA Paper 73-996, Oct. 1973.

19. Davis, Sanford S.: Theory of Discrete Vortex Noise. AIAA J., vol. 13,
       no. 3, March 1975, pp. 375-380.

20. Tijdeman, H.; and Zwaan, R. J.: On the Prediction of Aerodynamic Loads
       on Oscillating Wings in Transonic Flow. Report 612, AGARD, 1974.

TABLE 1.- DSMA 523 PROFILE COORDINATES

$\frac{z}{c}$	$\frac{z_{upper}}{c}$	$\frac{z_{lower}}{c}$	$\frac{z}{c}$	$\frac{z_{upper}}{c}$	$\frac{z_{lower}}{c}$
0.000500	0.005069	-0.005096	0.440000	0.055247	-0.053009
.001000	.007096	-.007128	.460000	.055146	-.052143
.002500	.011063	-.011078	.480000	.054973	-.051136
.005000	.015320	-.015320	.500000	.054723	-.049915
.007500	.018417	-.018417	.520000	.054390	-.048483
.010000	.020716	-.020671	.540000	.053976	-.046780
.012500	.022651	-.022548	.560000	.053486	-.044613
.015000	.024267	-.024135	.580000	.052917	-.042006
.020000	.026918	-.026744	.600000	.052269	-.038885
.030000	.030729	-.030667	.620000	.051540	-.035181
.040000	.033459	-.033607	.640000	.050726	-.030940
.060000	.037407	-.038087	.660000	.049826	-.026390
.080000	.040367	-.041739	.680000	.048832	-.021541
.100000	.042987	-.044548	.700000	.047725	-.016958
.120000	.045198	-.046796	.720000	.046494	-.012692
.140000	.047017	-.048616	.740000	.045130	-.008750
.160000	.048543	-.050114	.760000	.043625	-.005200
.180000	.049828	-.051348	.780000	.041942	-.002041
.200000	.050902	-.052370	.800000	.040043	.000686
.220000	.051802	-.053207	.820000	.037907	.002965
.240000	.052563	-.053890	.840000	.035502	.004757
.260000	.053199	-.054423	.860000	.032780	.006021
.280000	.053729	-.054808	.880000	.029666	.006687
.300000	.054161	-.055056	.900000	.026155	.006606
.320000	.054513	-.055163	.920000	.022185	.005630
.340000	.054788	-.055137	.940000	.017708	.003565
.360000	.054998	-.054978	.960000	.012642	.000348
.380000	.055149	-.054701	.980000	.006842	-.004210
.400000	.055240	-.054283	1.000000	.000308	-.010109
.420000	.055272	-.053719	$R_{le}/c = 0.023$		

21

Blank
Page
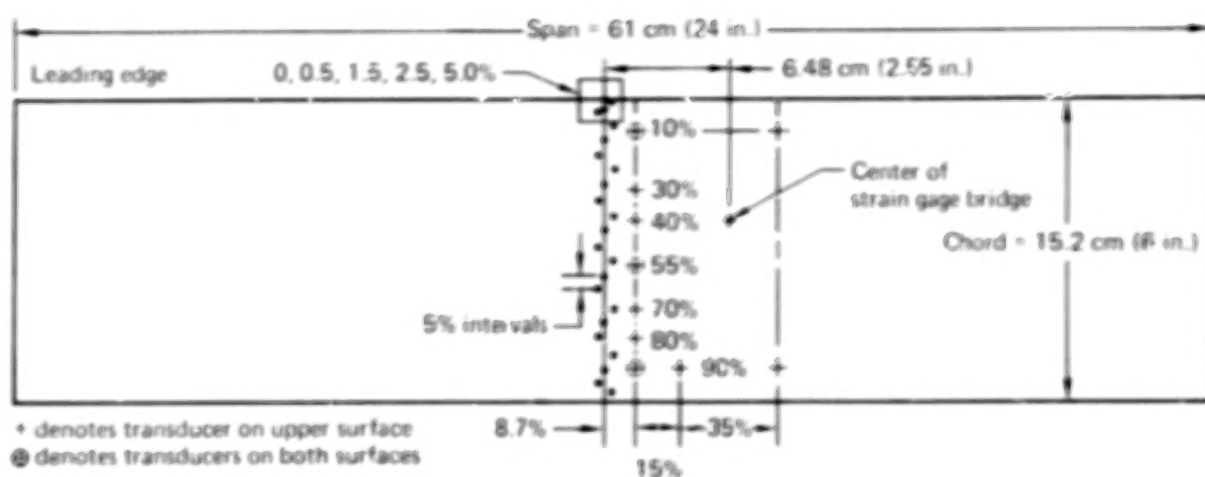
Figure 1.- Locations of 13 pressure transducers, a strain gage bridge for bending moment, and the primary row of static pressure orifices on model. Dimensions in percent chord unless otherwise specified.
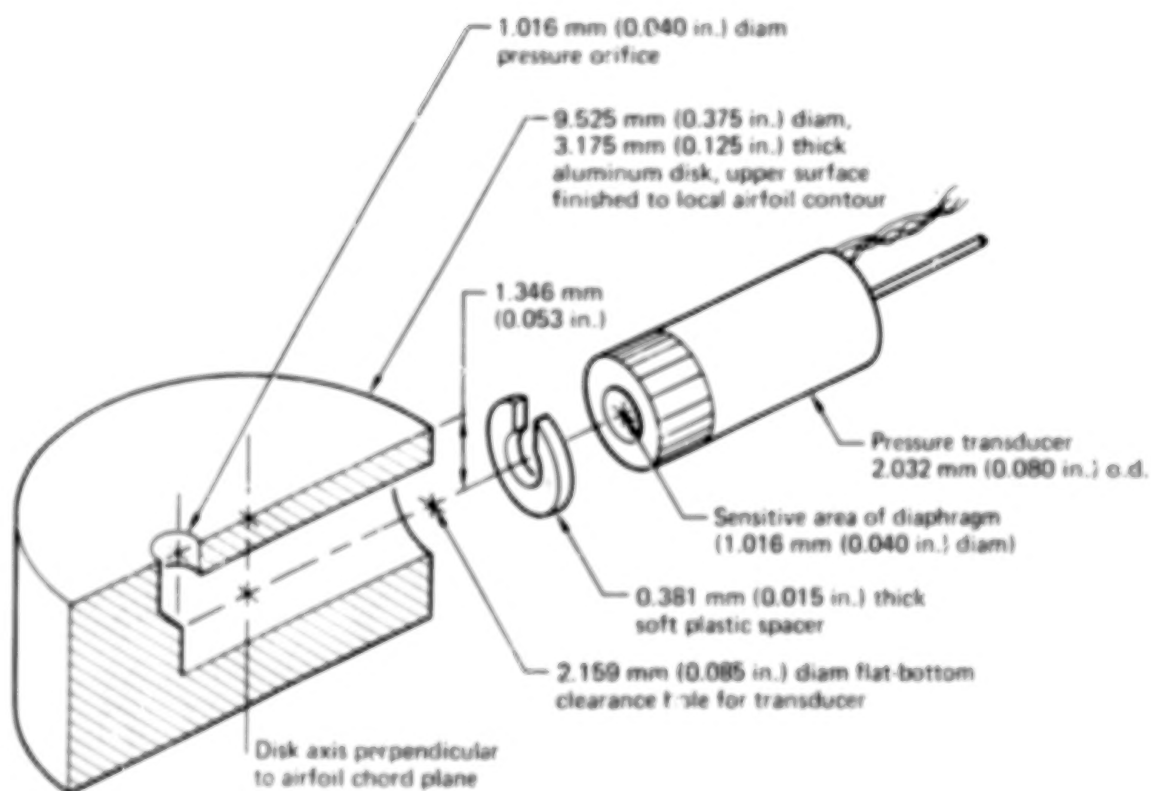
Figure 2.- Partial section view illustrating pressure transducer installation.
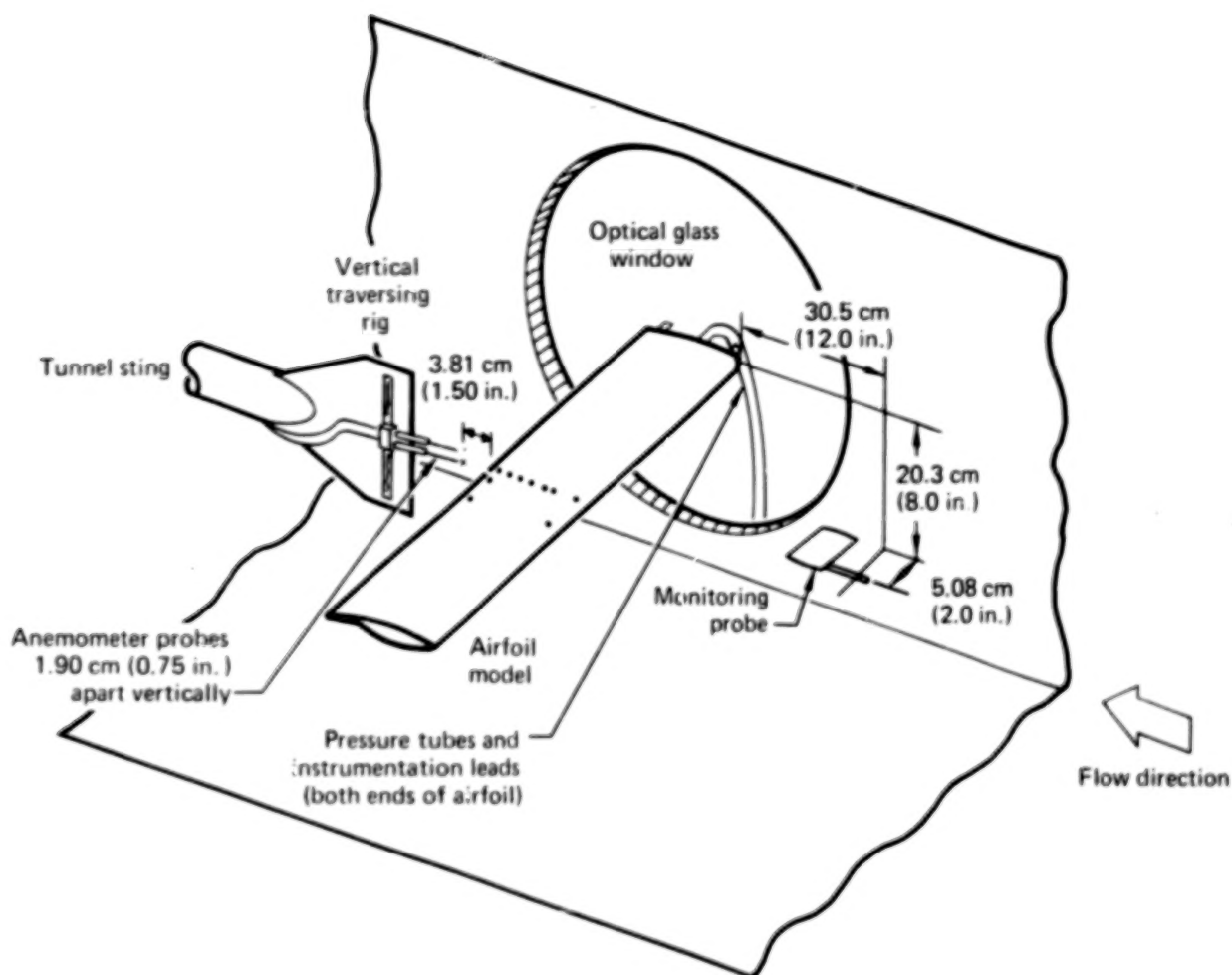
Figure 3.- Sketch of test section setup for dynamic measurements.

Labels within figure:
- Optical glass window
- Vertical traversing rig
- Tunnel sting
- 3.81 cm (1.50 in.)
- 30.5 cm (12.0 in.)
- 20.3 cm (8.0 in.)
- 5.08 cm (2.0 in.)
- Monitoring probe
- Anemometer probes 1.90 cm (0.75 in.) apart vertically
- Airfoil model
- Pressure tubes and instrumentation leads (both ends of airfoil)
- Flow direction
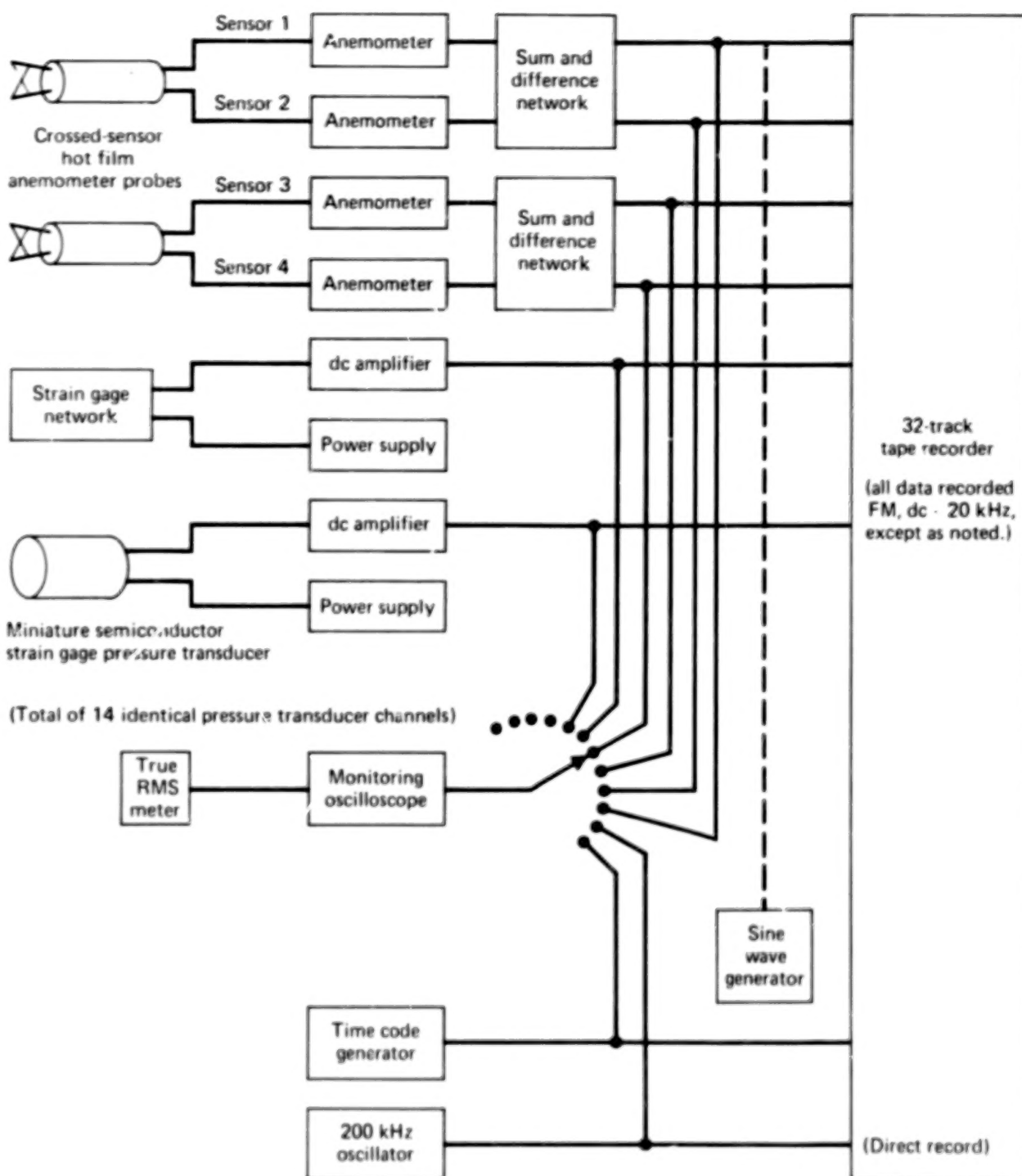
Figure 4.- Block diagram of instrumentation for acquisition and recording of dynamic data.
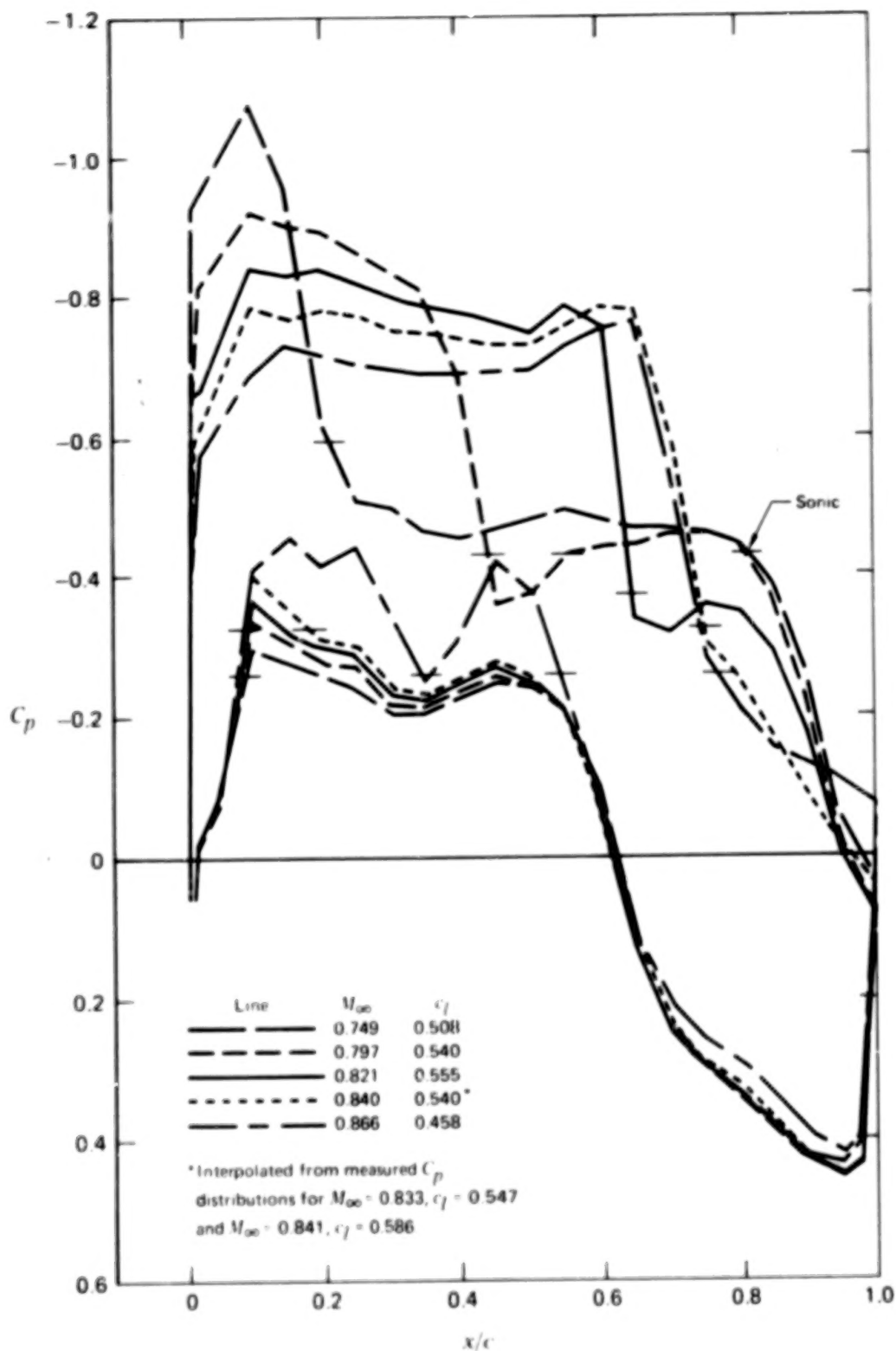
Figure 5.- Development of airfoil pressure distribution with increasing M_∞ at approximately constant c_1, $Re_c = 2\times10^6$.
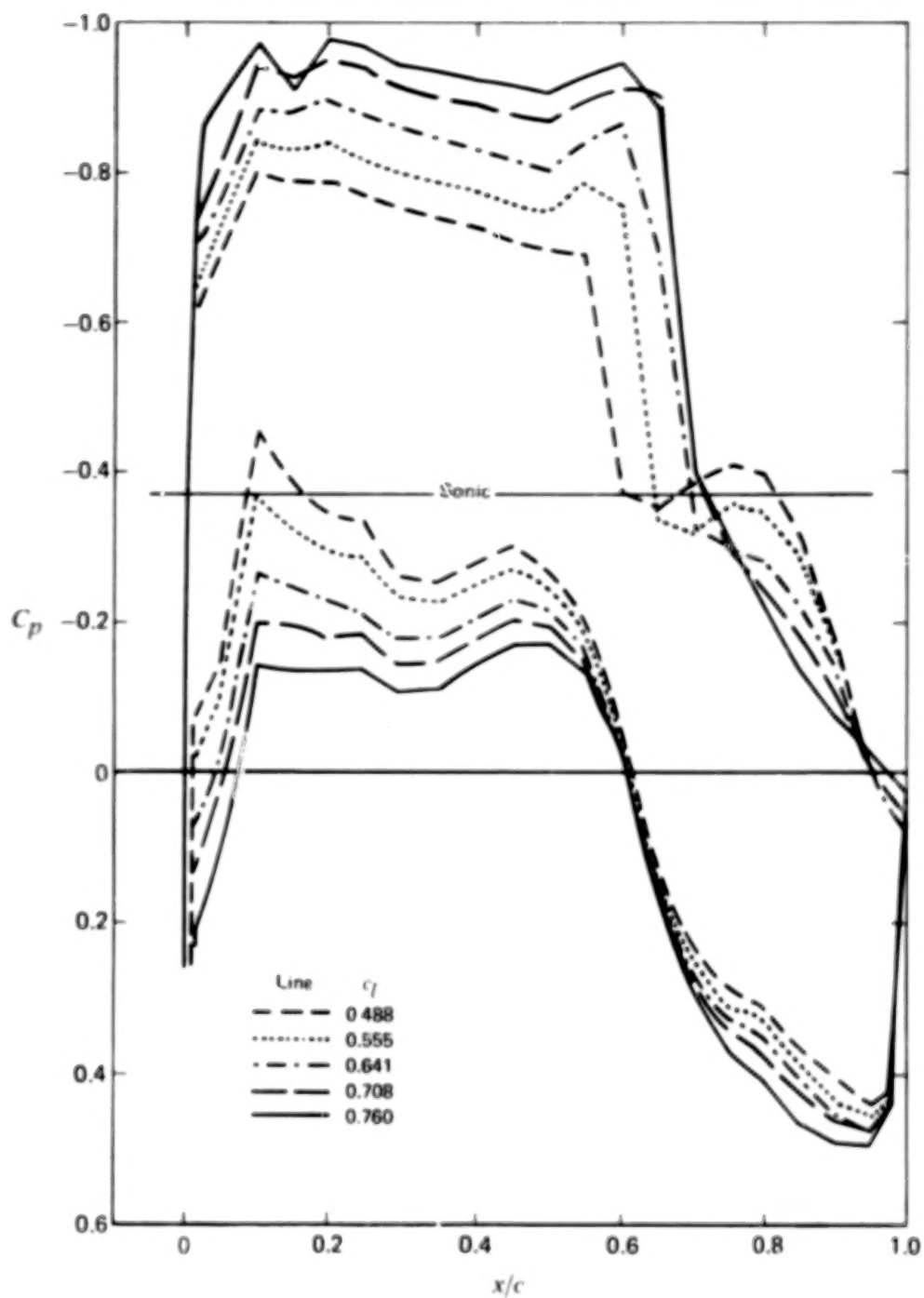
Figure 6.- Evolution with increasing c_l of airfoil pressure distribution at $M_\infty = 0.82$, $Re_c = 2\times10^6$.

a) $M_\infty = 0.75$, $c_l = 0.51$

d) $M_\infty = 0.83$, $c_l = 0.54$

b) $M_\infty = 0.82$, $c_l = 0.53$

e) $M_\infty = 0.84$, $c_l = 0.57$

c) $M_\infty = 0.82$, $c_l = 0.64$
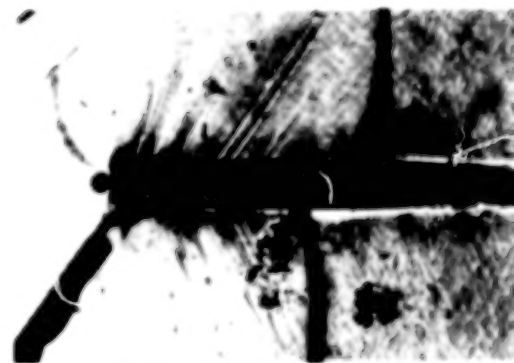
f) $M_\infty = 0.86$, $c_l = 0.49$

Figure 7.- Development of flow field with variations in M_∞ and c_l ($Re_c = 3\times10^6$ except in (c), where $Re_c = 2\times10^6$).
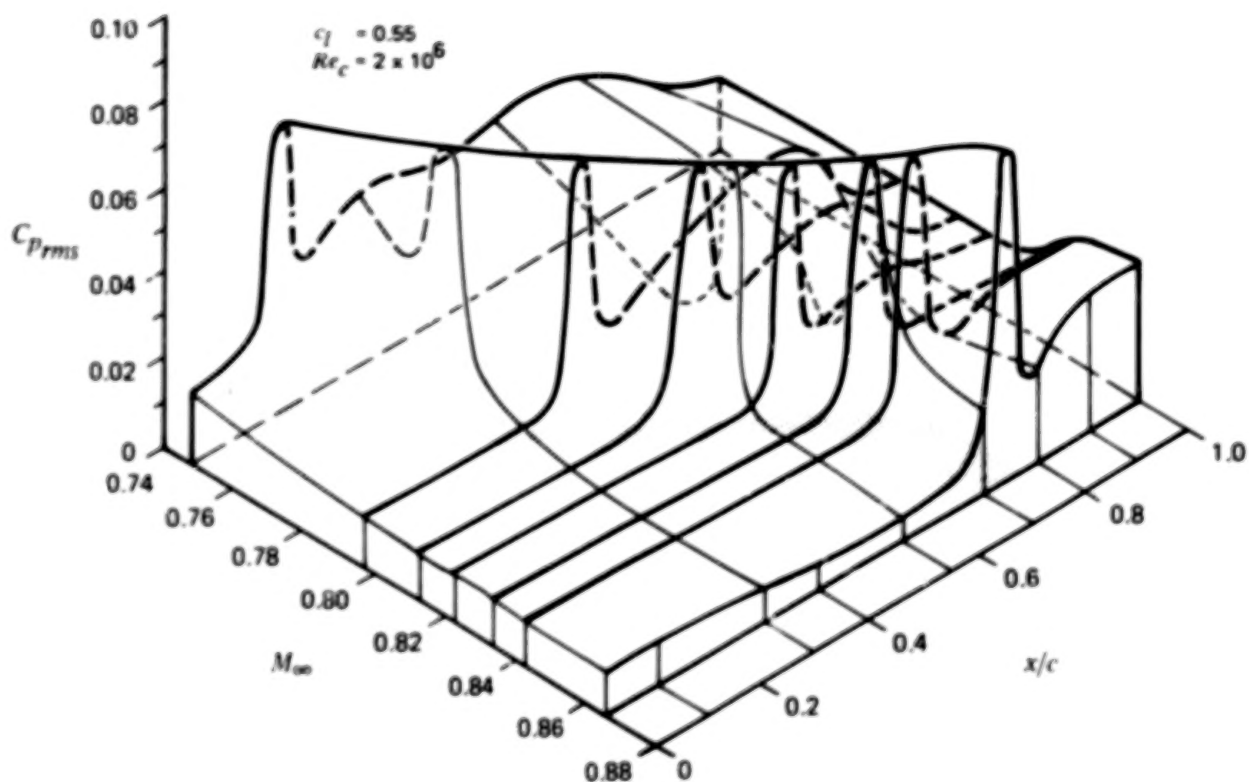
Figure 8.- Chordwise fluctuating pressure distribution: evolution with Mach number variation (shaded area indicates location of shock region).
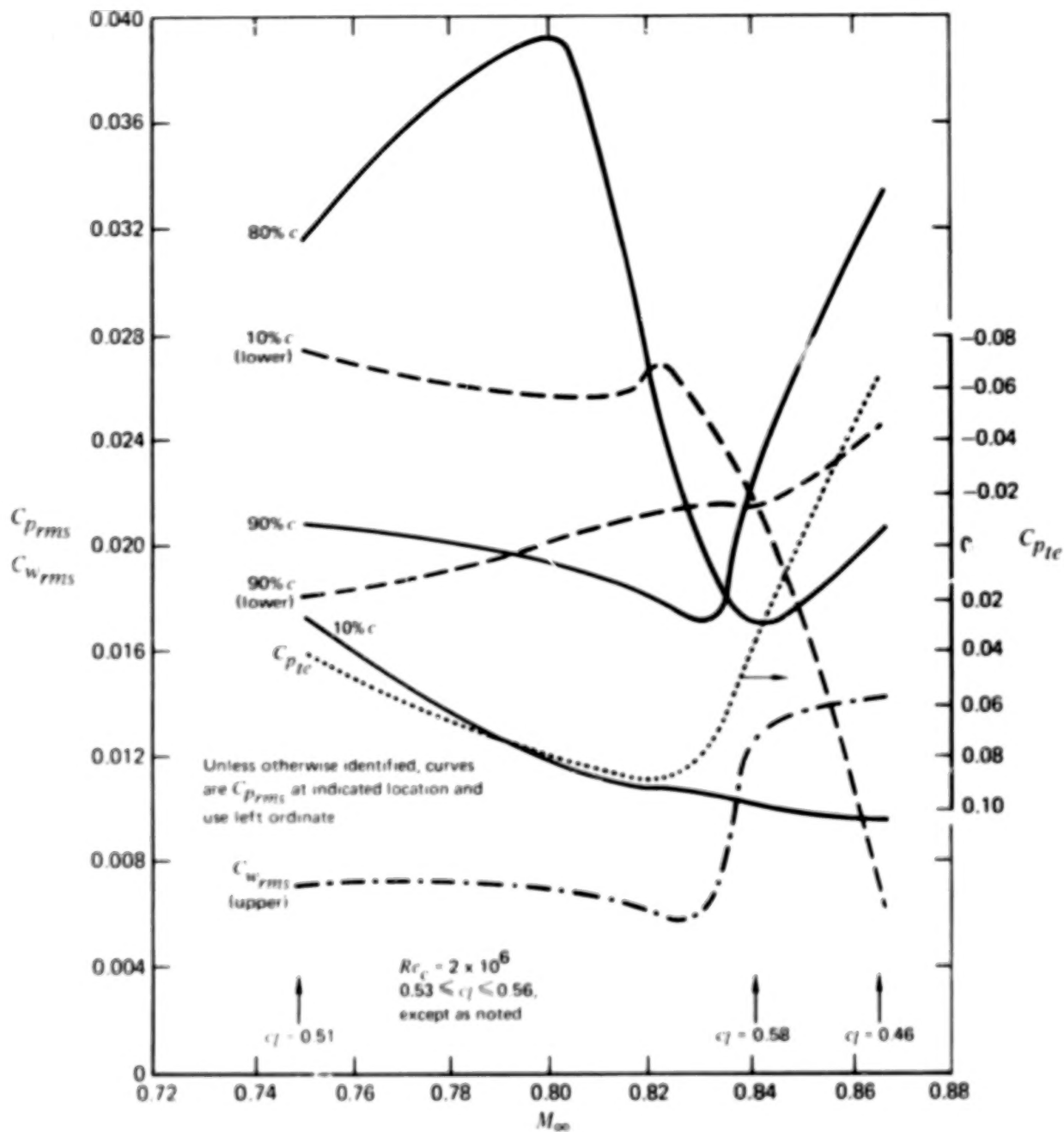
Figure 9.- Variation of $C_{p_{rms}}$, $C_{w_{rms}}$, and $C_{p_{te}}$ with increasing M_∞.
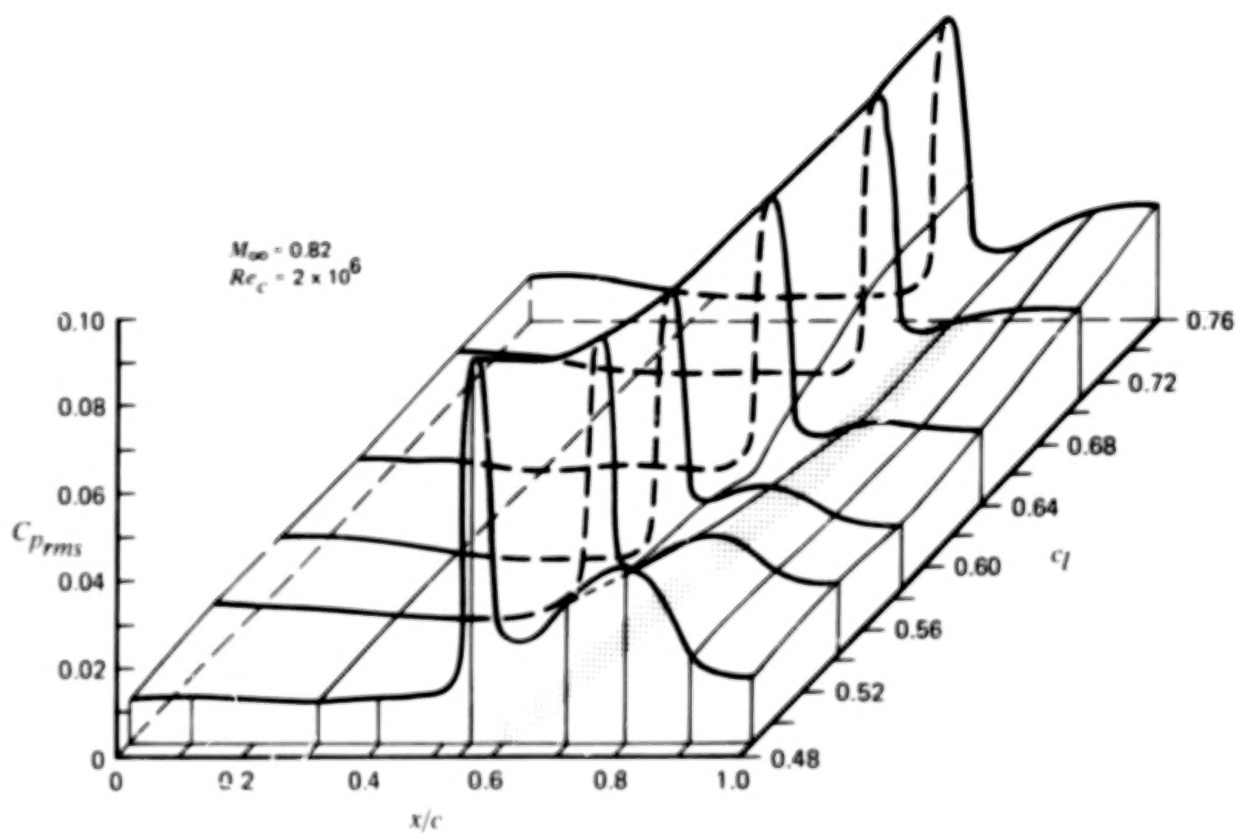
Figure 10.- Chordwise fluctuating pressure distribution: variation with increasing lift (shaded area indicates shock region).
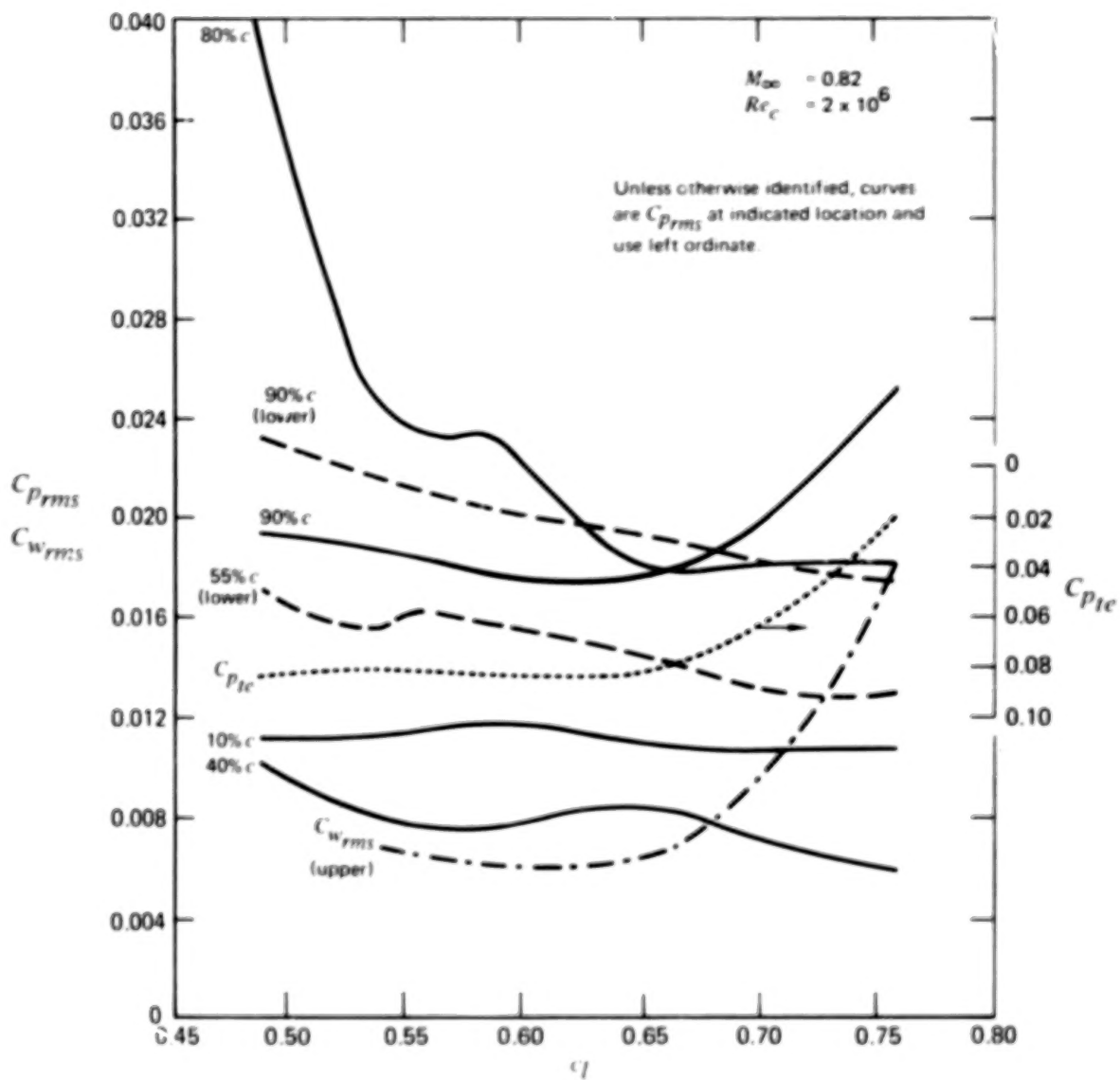
Figure 11.- Variation of $C_{w_{rms}}$, $C_{p_{rms}}$, and $C_{p_{te}}$ with increasing c_l.
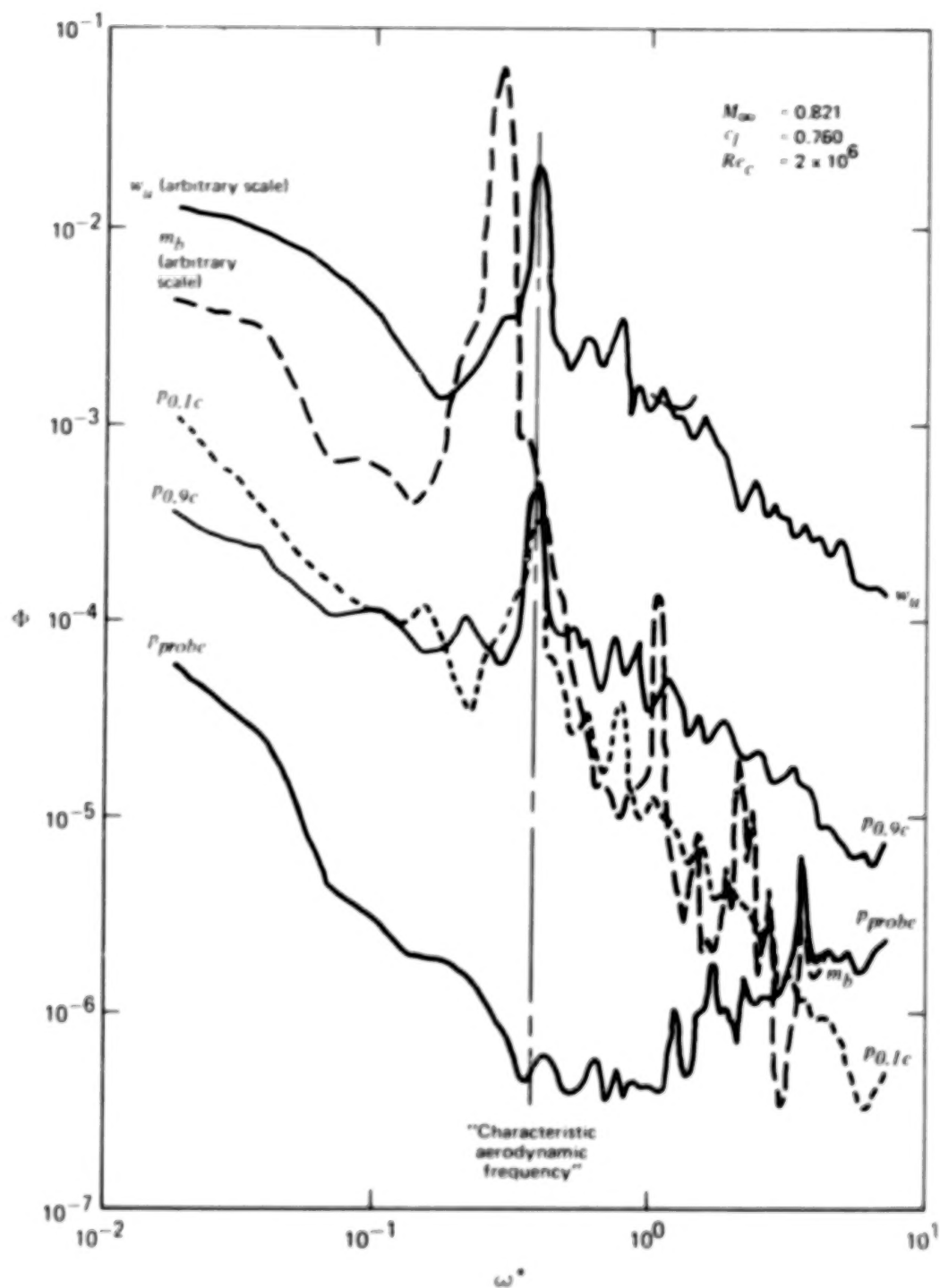
Figure 12.- Independence of flow-field fluctuations and airfoil bending vibrations.
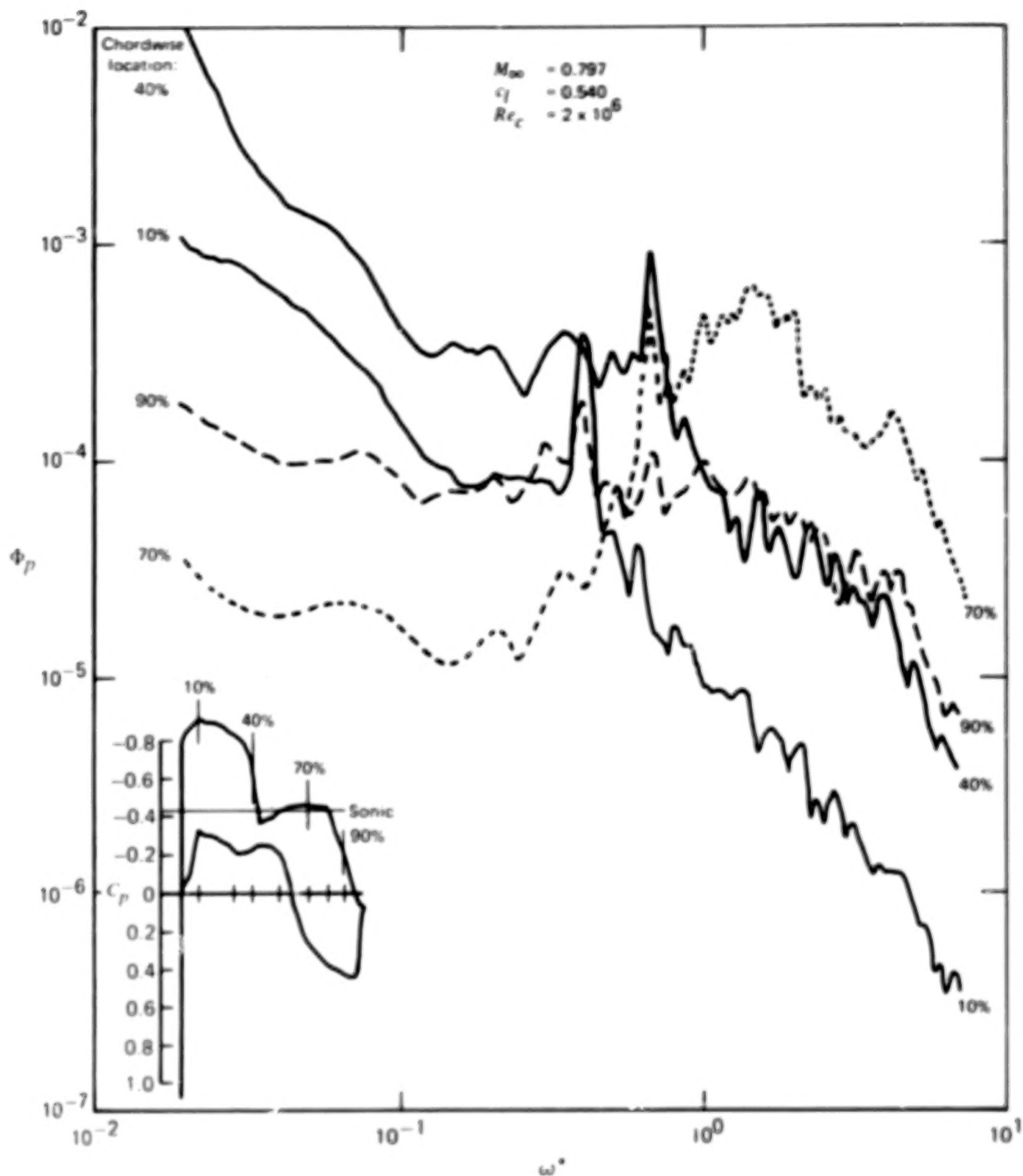
Figure 13.- Chordwise variation of upper surface fluctuating pressure power spectra (M_∞ = 0.797).

34
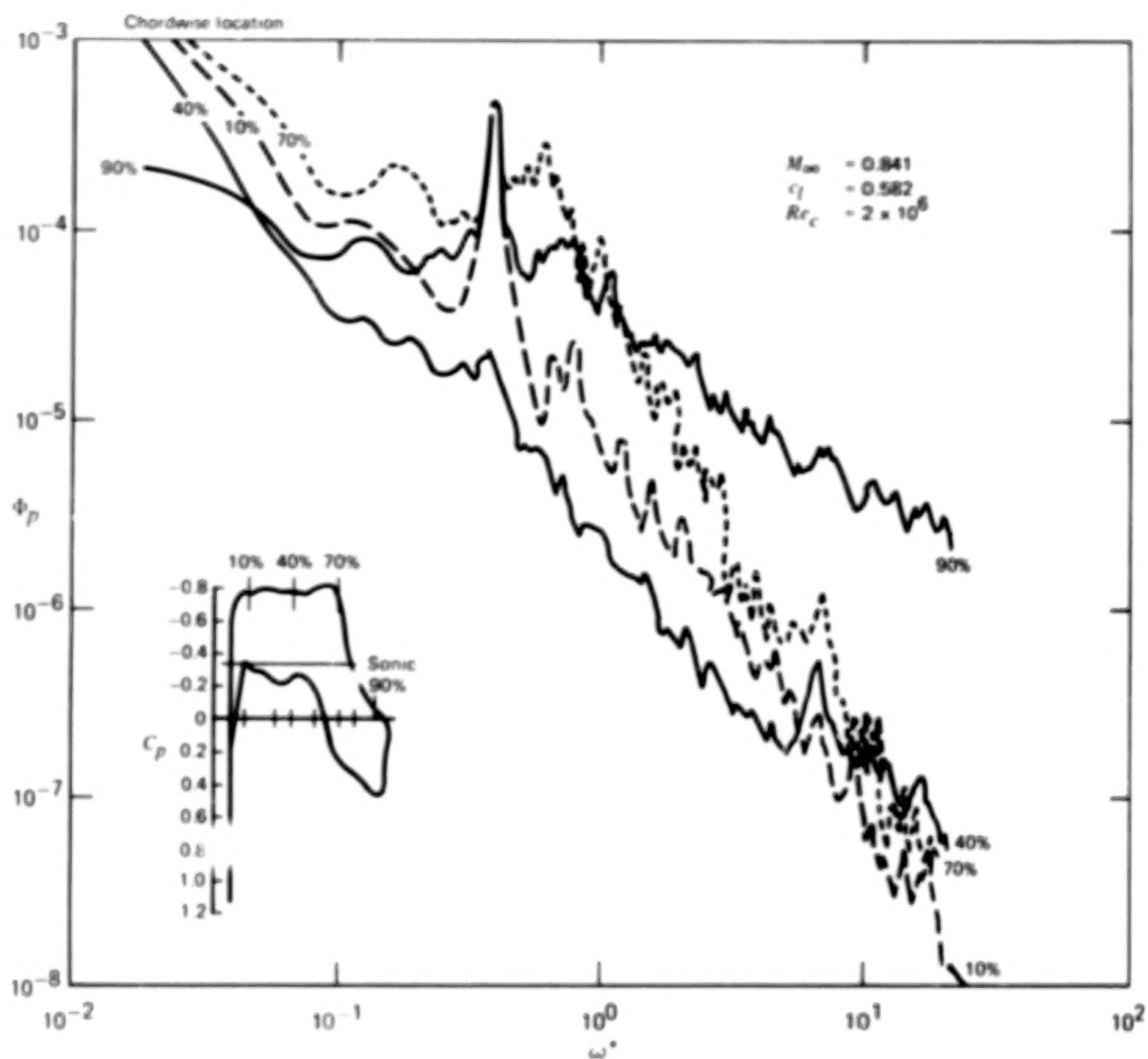
Figure 14.- Chordwise variation of upper surface fluctuating pressure power spectra (M_∞ = 0.841).
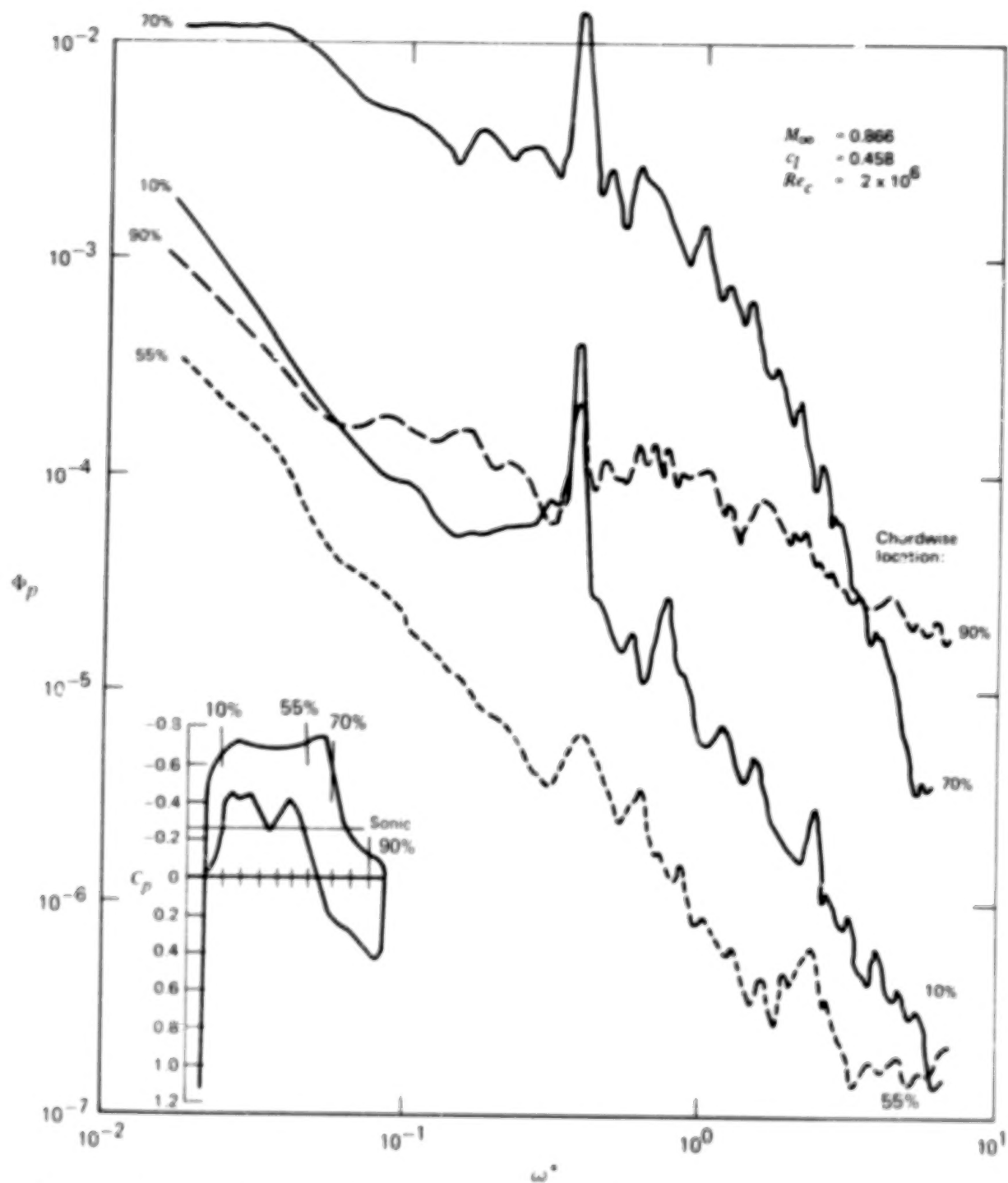
Figure 15.- Chordwise variation of upper surface fluctuating pressure power spectra (M_∞ = 0.866).
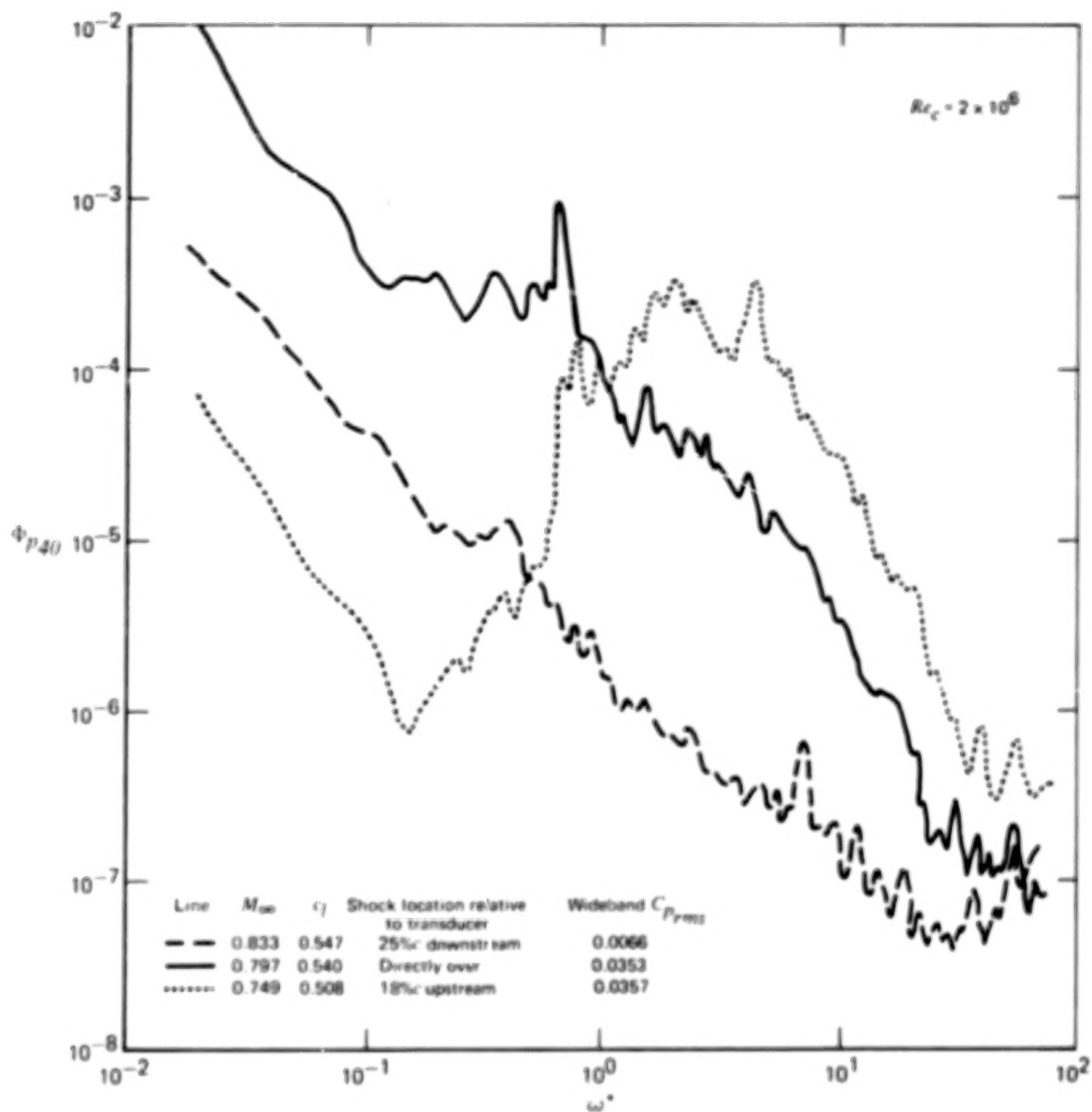
Figure 16.- Surface pressure power spectra at 40-percent chord; dependence on relative shock position.
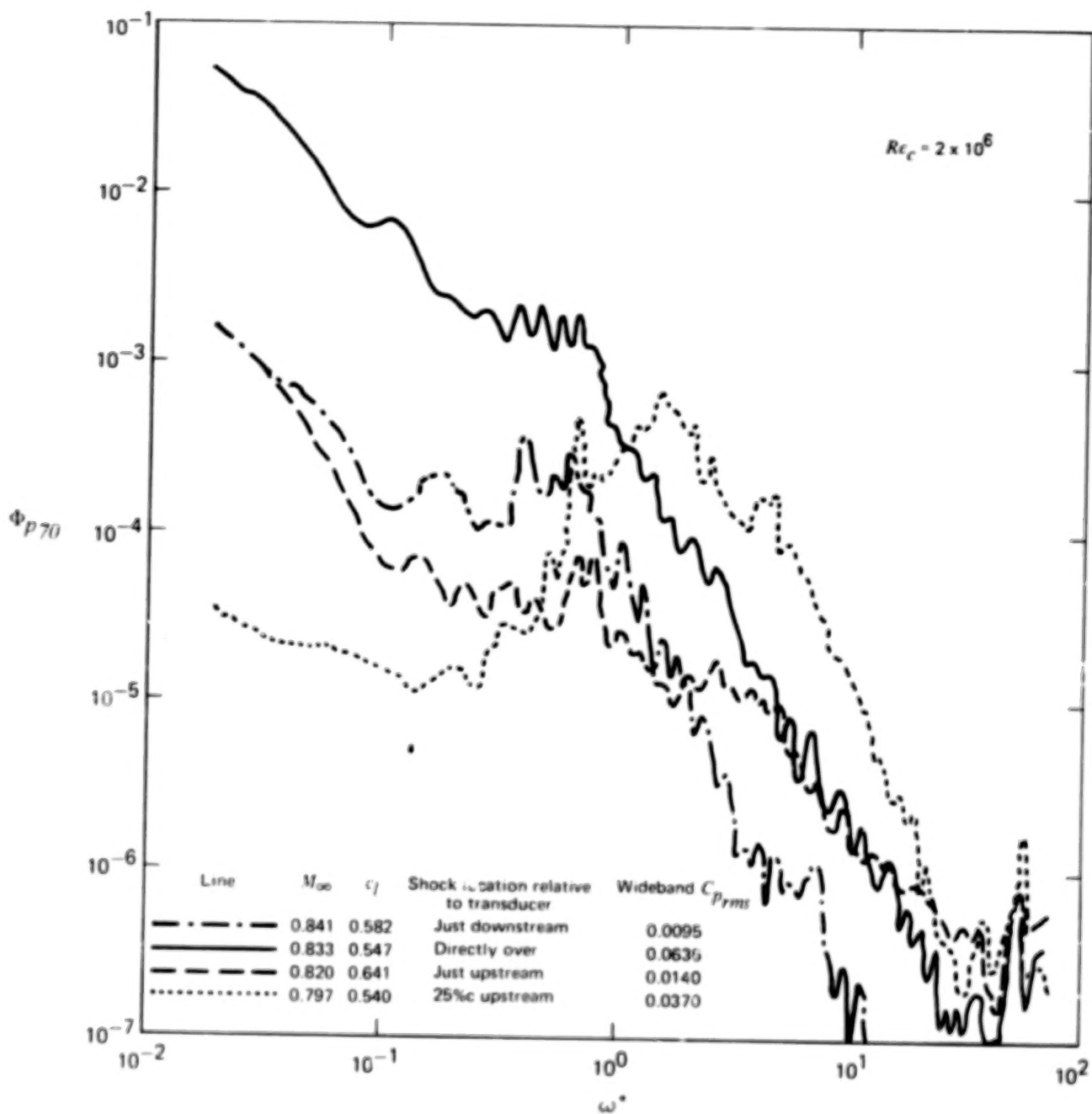
Figure 17.- Surface pressure power spectra at 70-percent chord; dependence on relative shock position.

Line	M_∞	c_l	Wideband $C_{P_{rms}}$	Comments on pressure distribution
— — —	0.75	0.51	0.0317	somewhat subsonic; long run of $\frac{\partial p}{\partial x} \approx 0$ aft of shock
— - — -	0.80	0.54	0.0391	reacceleration to supersonic aft of shock; 0.9 c $\approx$ sonic point
··········	0.82	0.56	0.0227	reacceleration to nearly sonic; $\frac{\partial p}{\partial x} \approx 0$ just ahead of 0.8 c
— — —	0.83	0.55	0.0185	slight easing of C_p rise aft of shock, but no reacceleration
——	0.87	0.46	0.0207	continued rapid C_p rise aft of shock; separation aft of 0.8 c

$Re_c = 2 \times 10^6$

$\Phi_{p_{80}}$

ω^*

Figure 18.- Surface pressure power spectra at 80-percent chord; relationship to local pressure distribution.

$Re_c = 2 \times 10^6$

Line	M_∞	c_l	$C_{p_{rms}}$	Trailing edge flow
	0.821	0.555	0.0169	Attached
	0.821	0.760	0.0249	Separated ~90%c
	0.841	0.582	0.0231	Separated ~90%c
	0.866	0.458	0.0336	Separated ~85%c

$\Phi_{p_{90}}$

ω^*
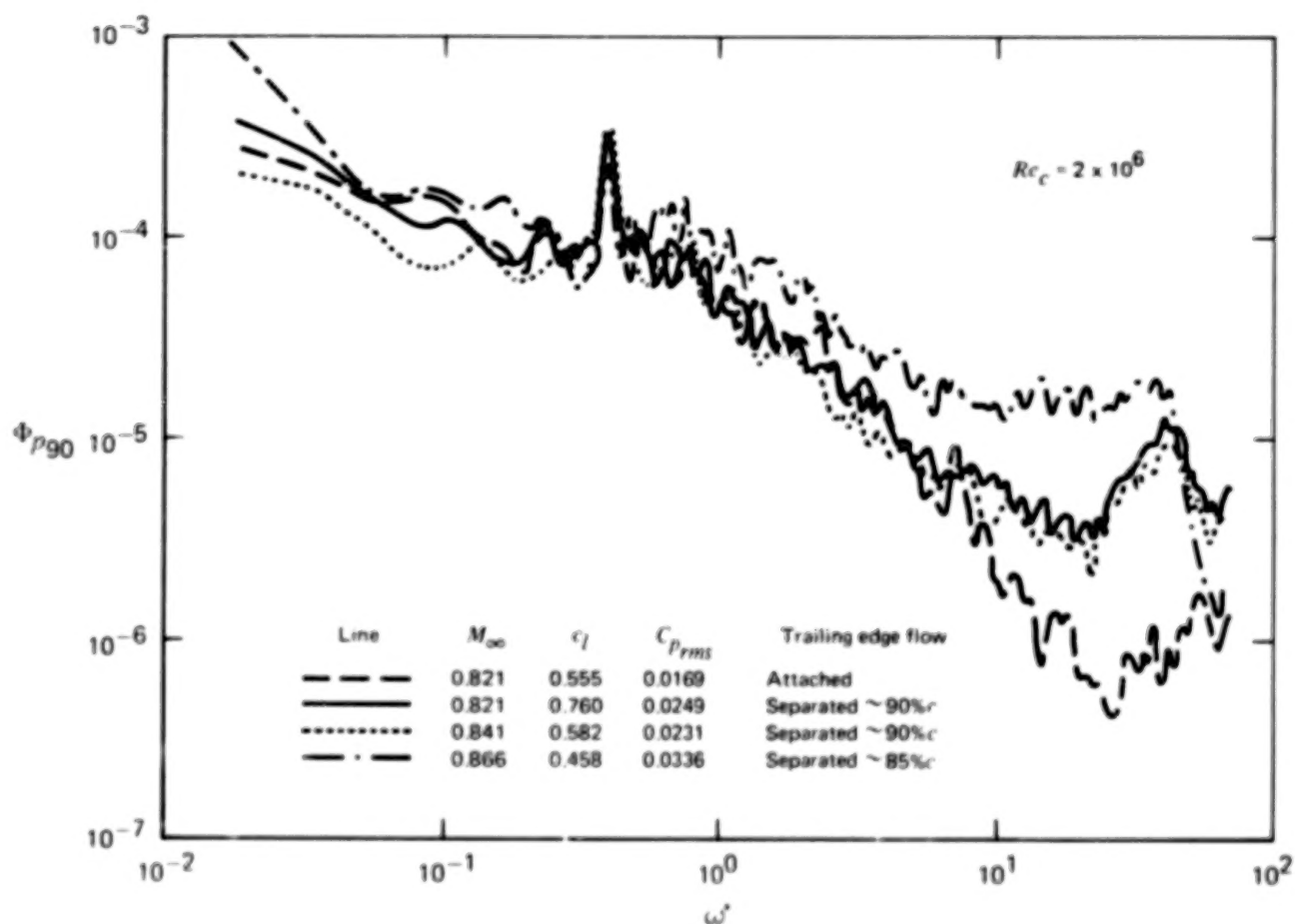
Figure 19.- Effect of trailing edge separation on surface pressure power spectra at 90-percent chord.
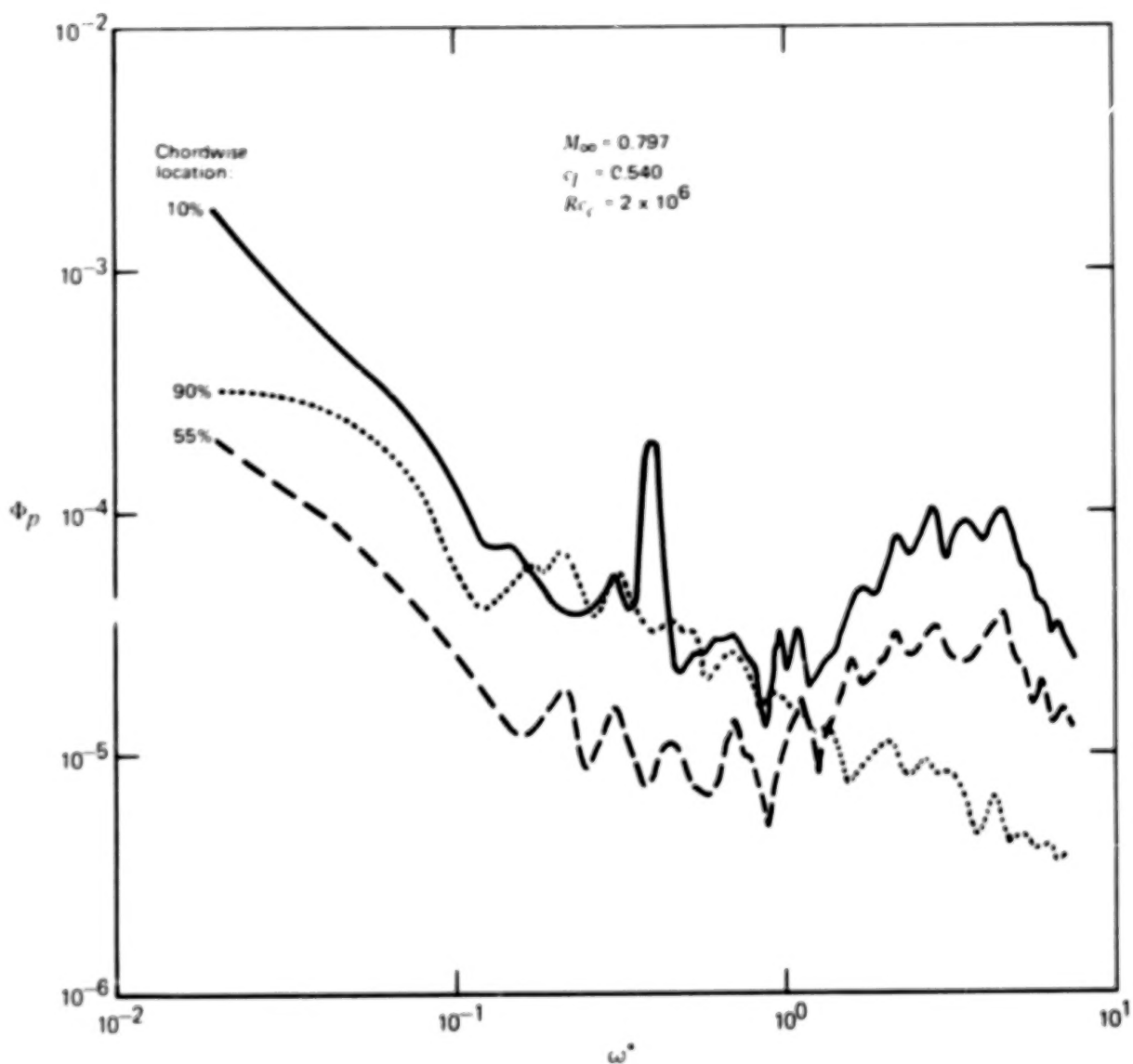
Figure 20.- Power spectra of pressure fluctuations on the airfoil lower surface for a typical flow condition.
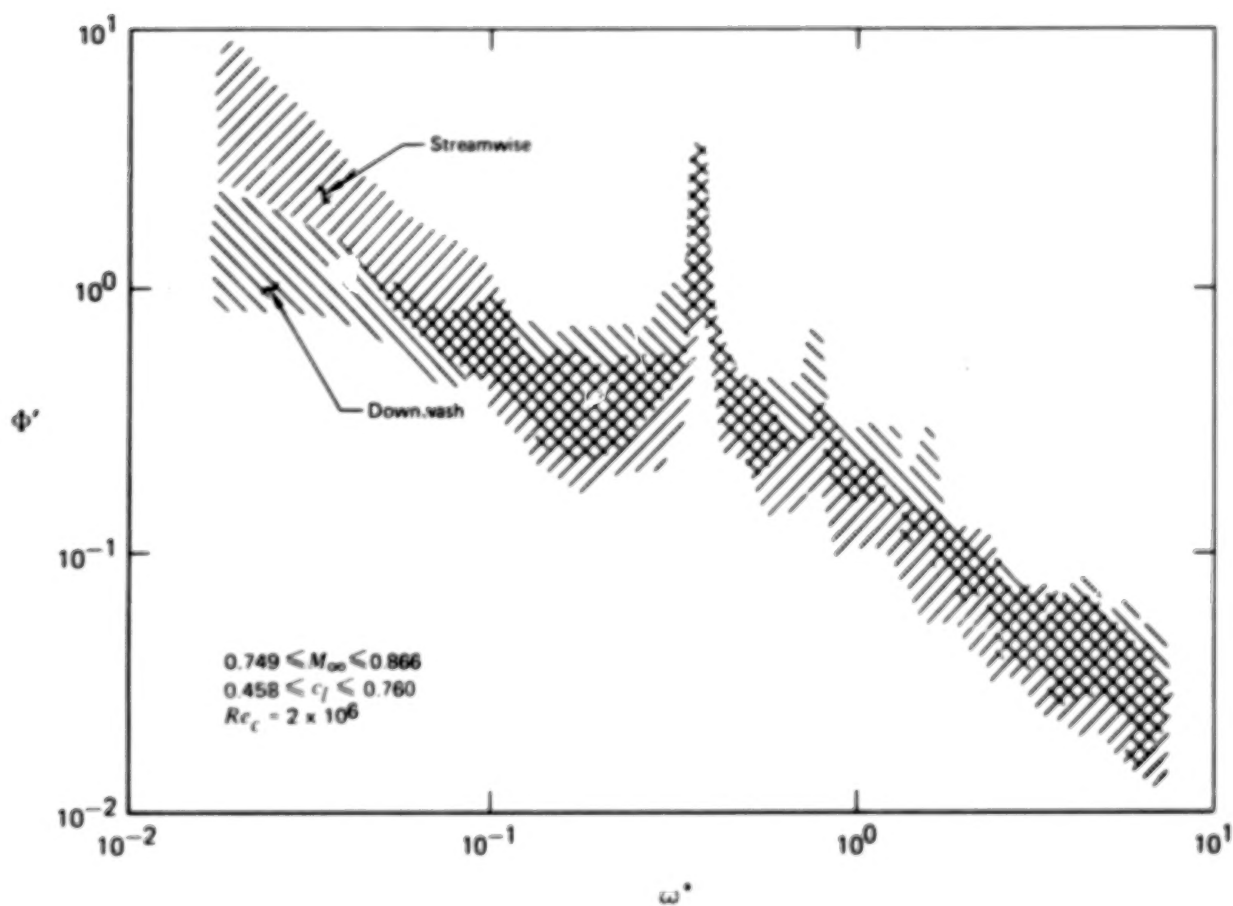
Figure 21.- Normalized power spectra of streamwise- and downwash-type
    fluctuations at upper edge of wake, 25-percent chord downstream of
    trailing edge.
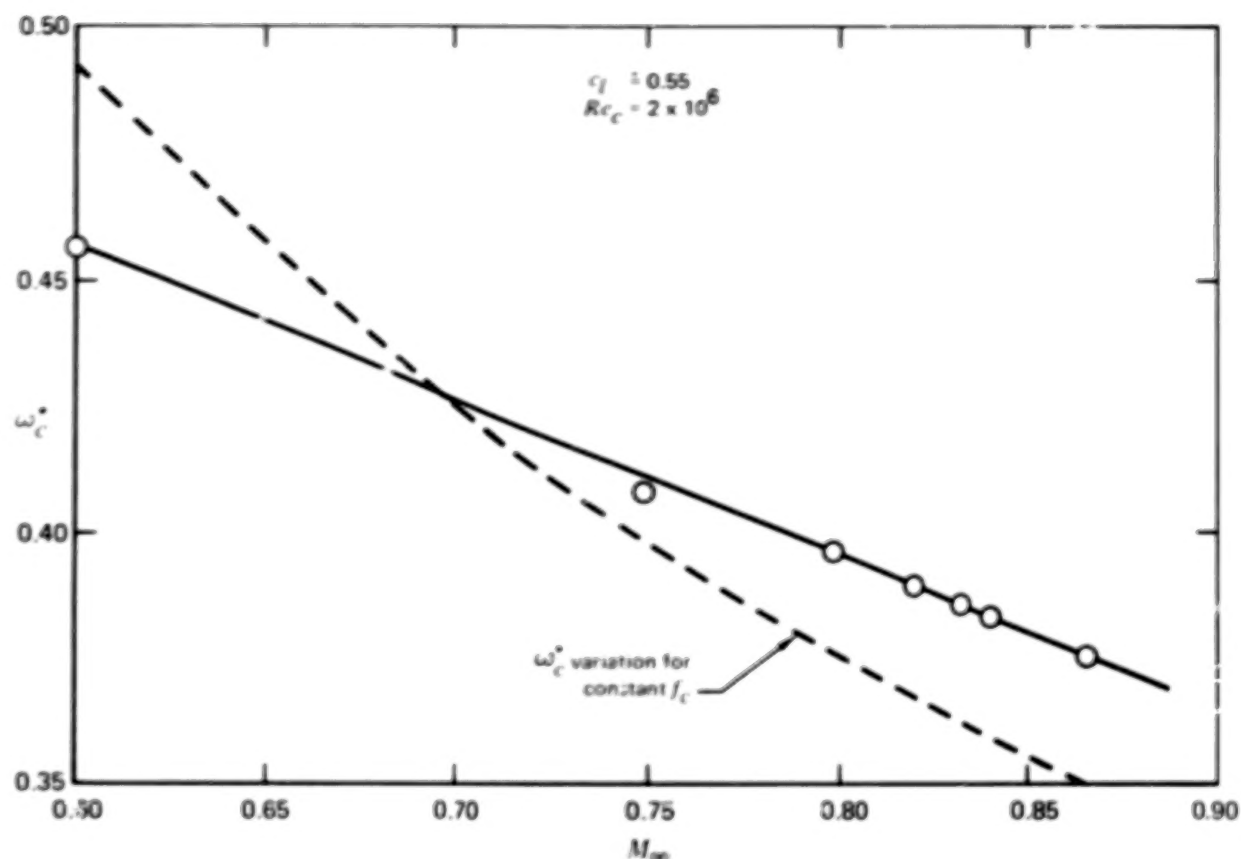
Figure 22.- Characteristic aerodynamic frequency as a function of M_∞.
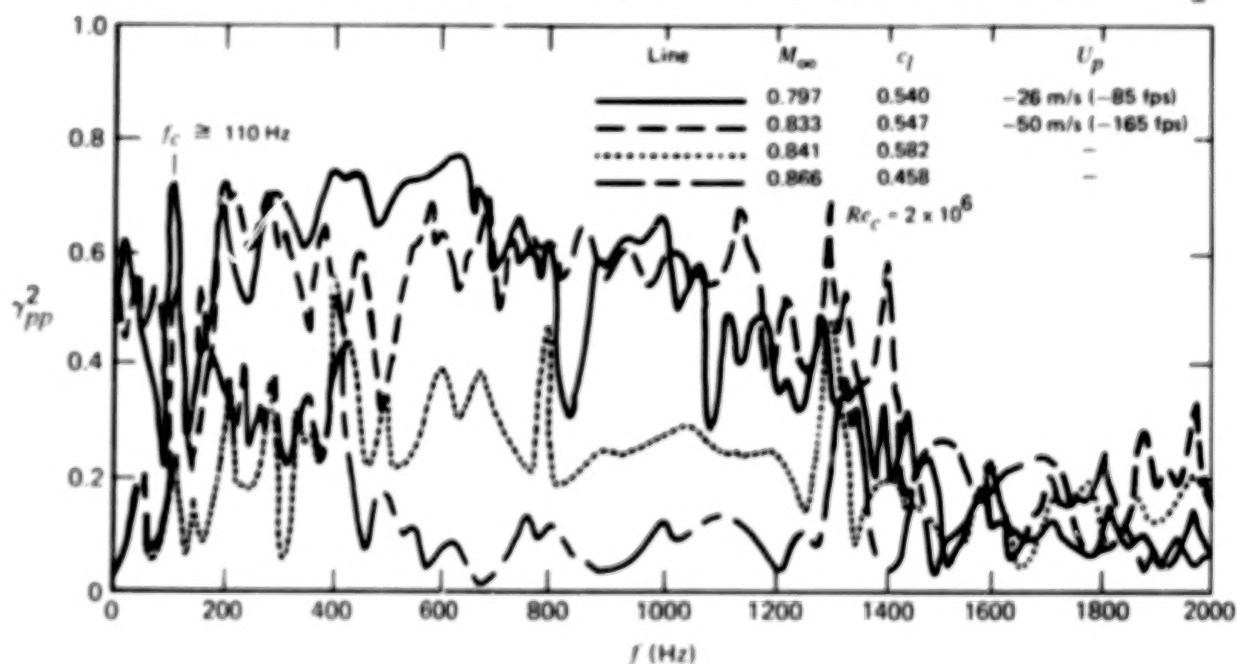
Figure 23.- Influence of Mach number on coherence of pressure fluctuations at 80-percent and 90-percent chord ($c_1 \doteq$ constant, $Re_c = 2\times10^6$).

Figure 24.- Pressure-pressure cross correlations illustrating the upstream
propagation of wide-band random disturbances downstream of the upper
surface shock.

Line	M_∞	c_l	Shock location	U_p
– – – –	0.749	0.508	upstream	−47 m/s (−155 fps)
·········	0.797	0.540	between	(180° out-of-phase)
———	0.821	0.555	downstream	−98 m/s (−320 fps)
– · – · –	0.833	0.547	downstream	–
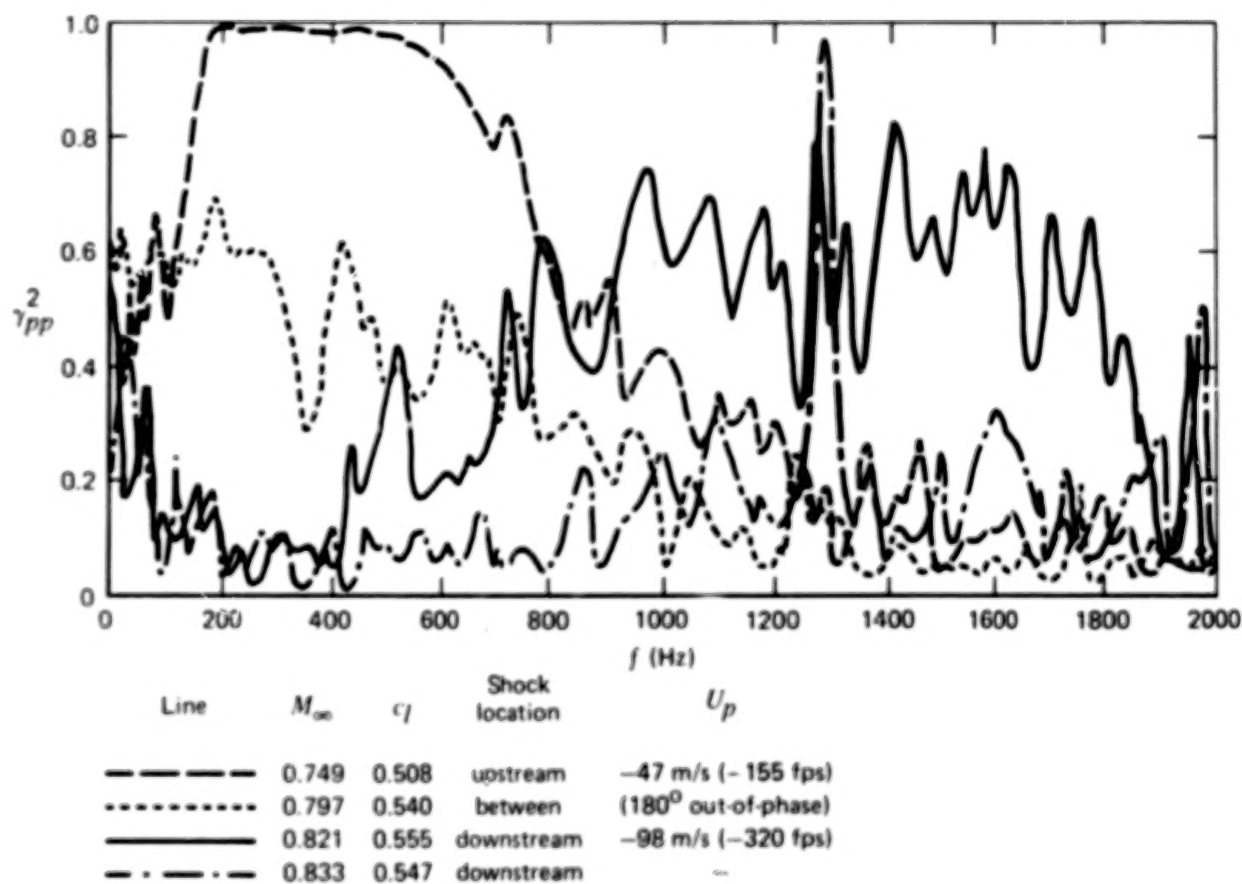
Figure 25.- Effect of Mach number and shock location variations on coherence of pressure fluctuations at 40-percent and 55-percent chord (c_l = constant, Re_c = 2×10^6).
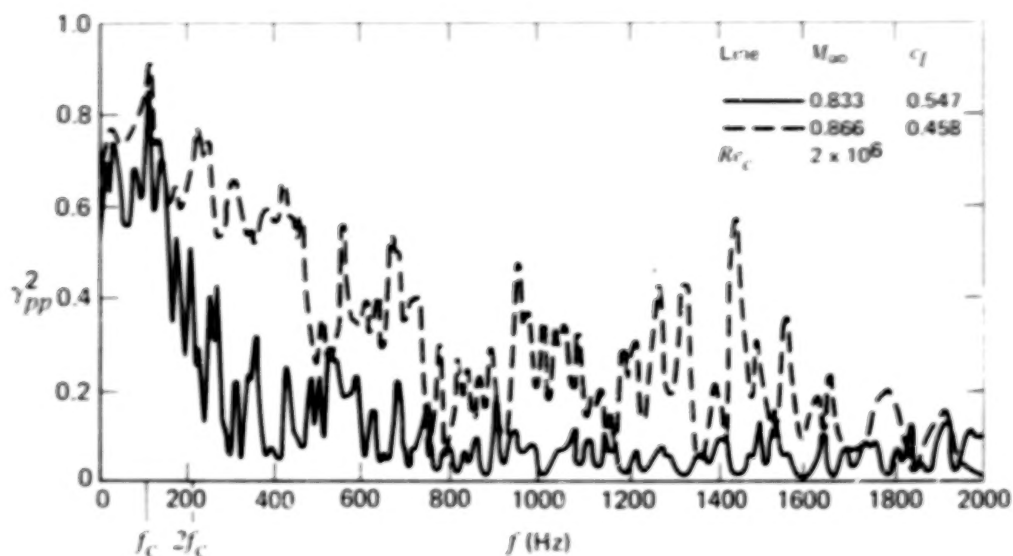
(a) Coherence functions.
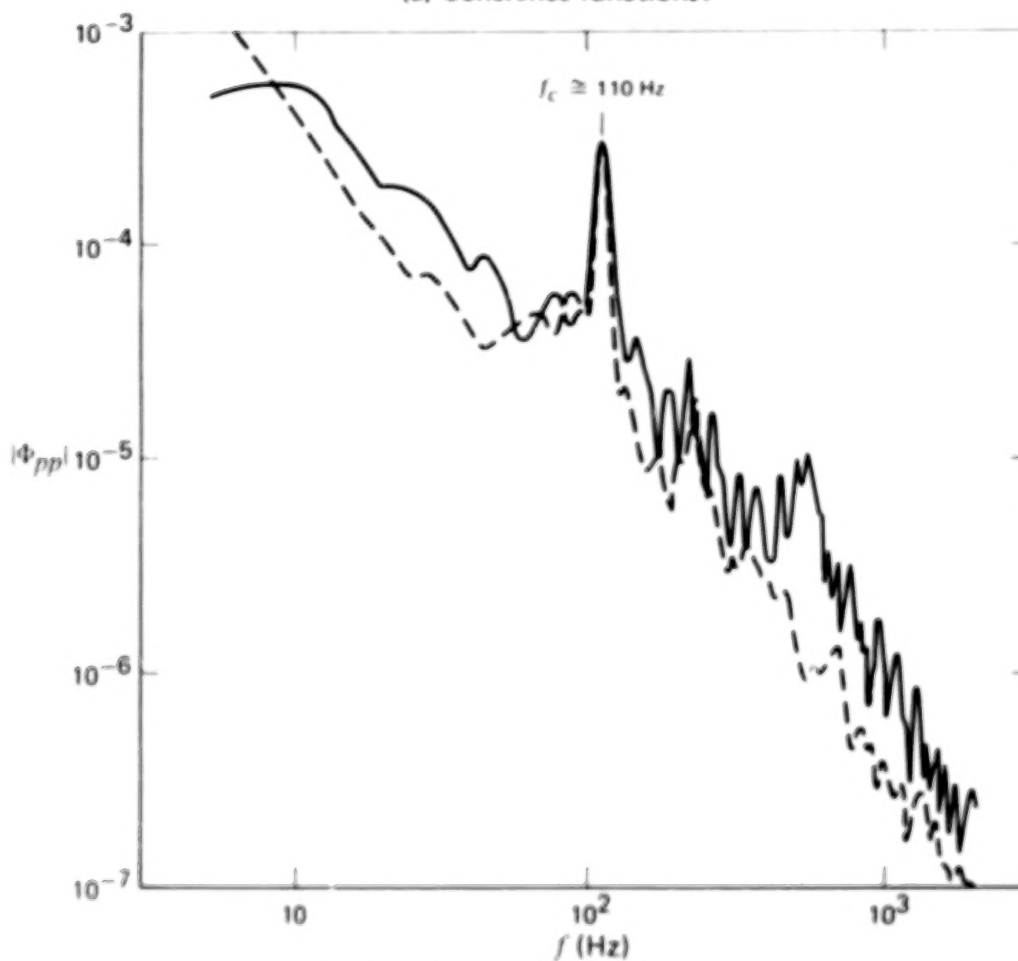
(b) Moduli of related cross-spectral densities.

Figure 26.- Coherence of pressure fluctuations at 10-percent chord on upper and lower surfaces of airfoil.
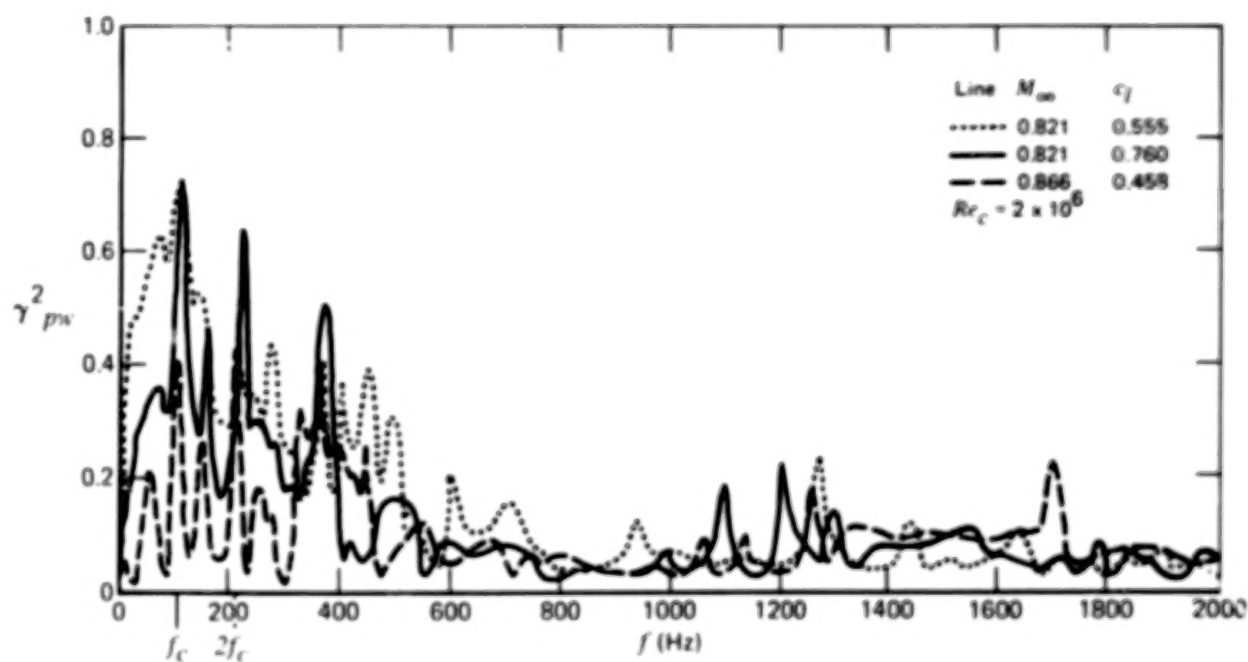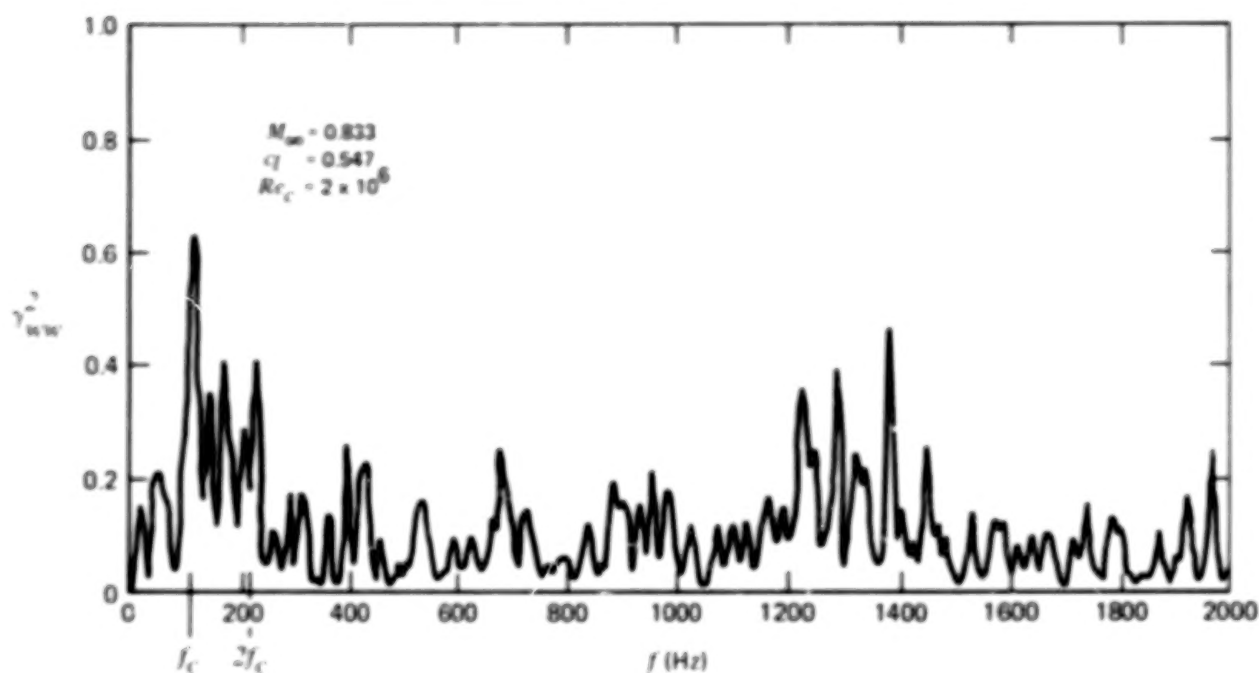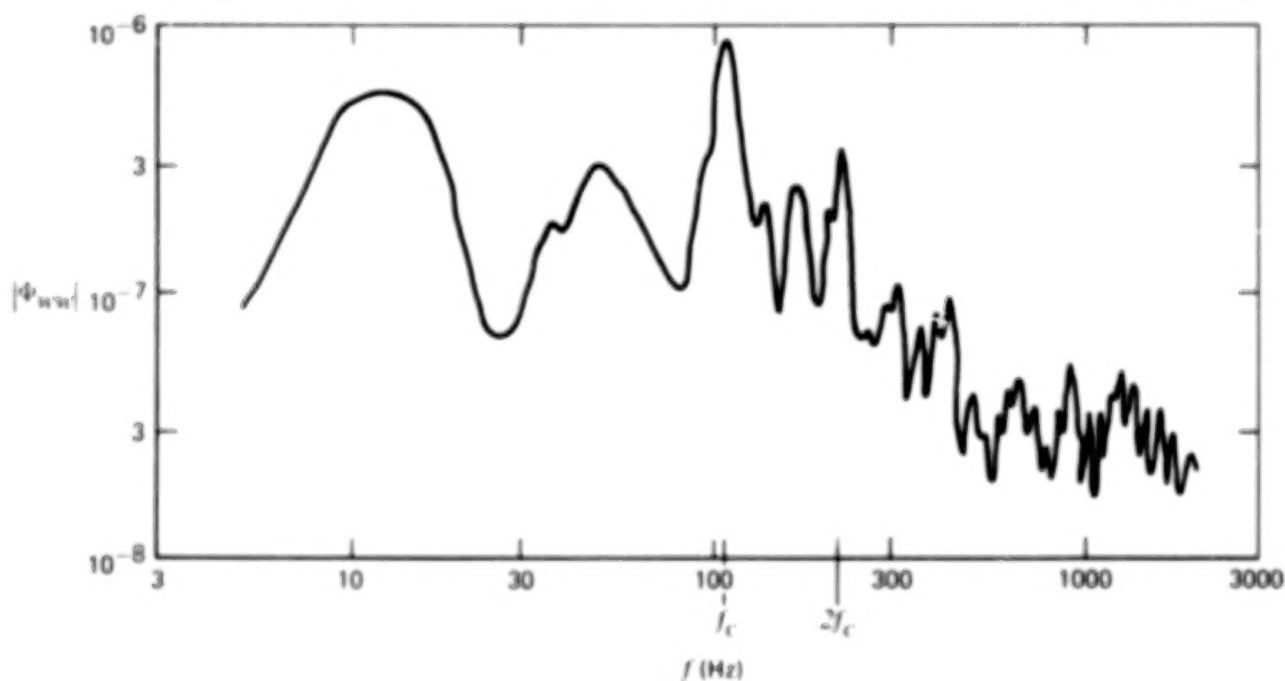
Figure 27.- Coherence of pressure fluctuations at 90-percent chord and downwash fluctuations at wake upper edge.

(a) Coherence function.

(b) Moduli of related cross-spectral densities.

Figure 26.- Coherence of pressure fluctuations at 10-percent chord on upper and lower surfaces of airfoil.
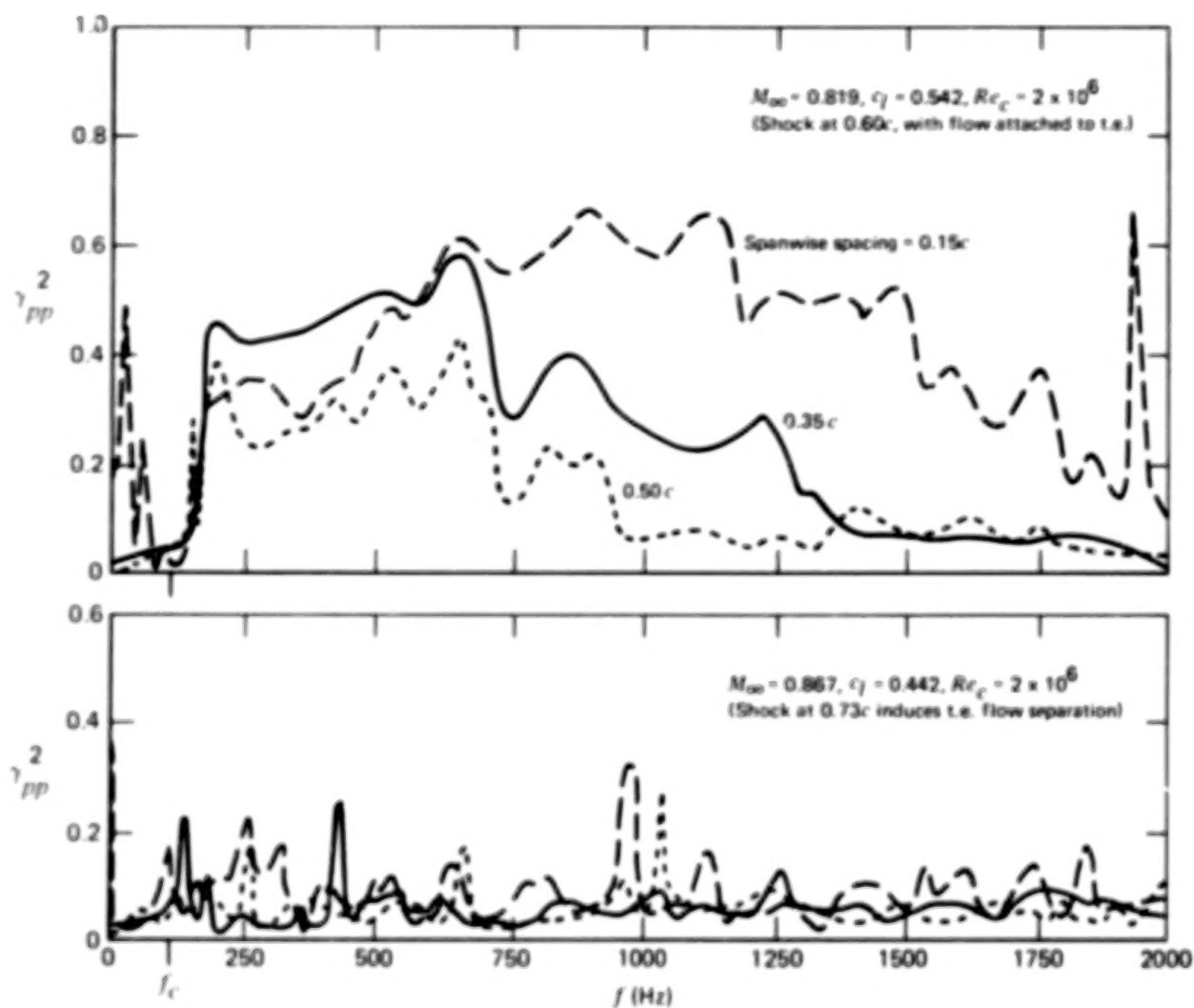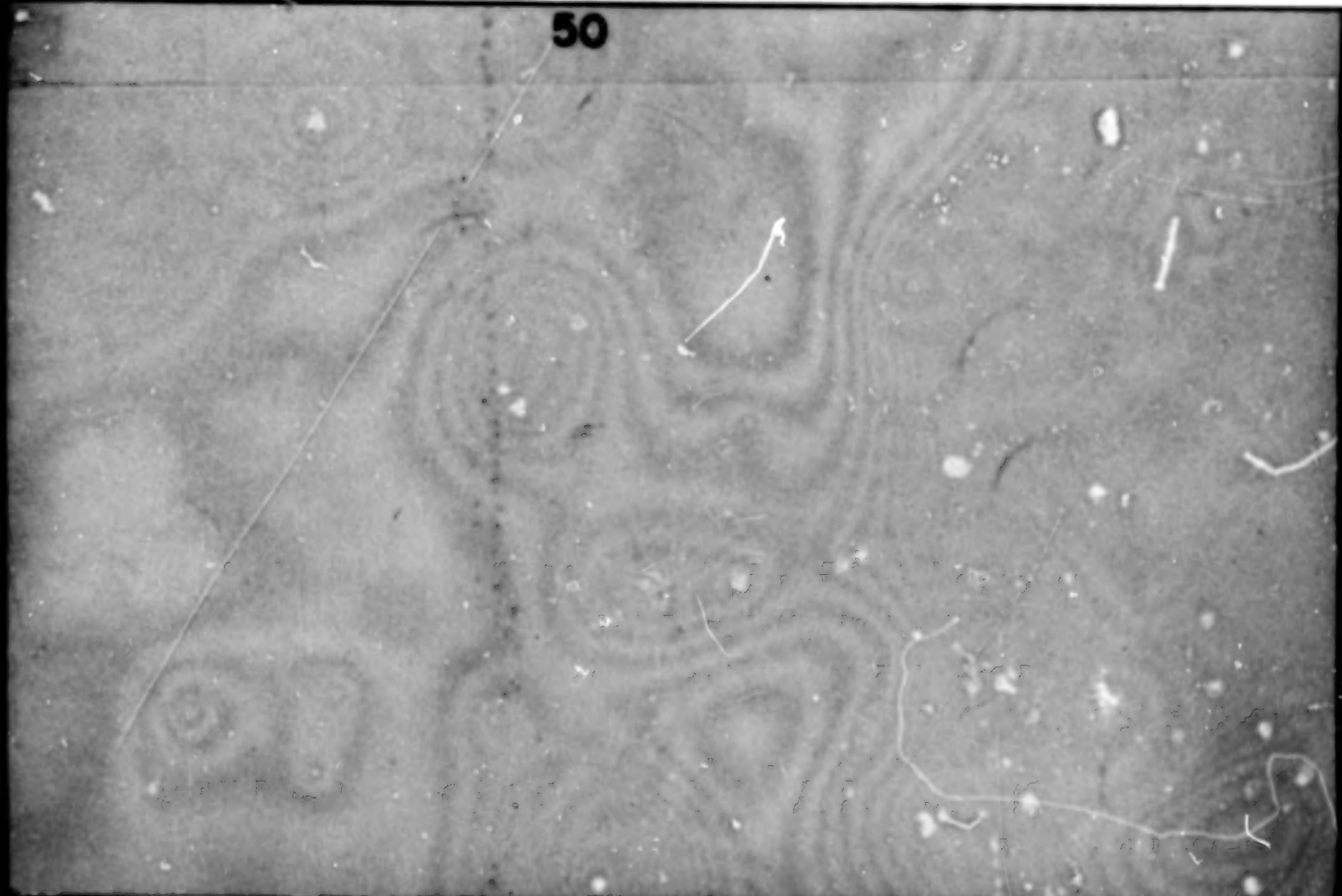
Figure 29.- Spanwise coherence of pressure fluctuations at 90-percent chord.

90
50

END

5.19 78